A Systematic Comparison of Tropical Waves over Northern Africa. Part II: Dynamics and Thermodynamics

ANDREAS SCHLUETER, ANDREAS H. FINK, AND PETER KNIPPERTZ

Institute of Meteorology and Climate Research, Karlsruhe Institute of Technology, Karlsruhe, Germany

(Manuscript received 2 October 2018, in final form 6 February 2019)

ABSTRACT

This study presents the first systematic comparison of the dynamics and thermodynamics associated with all major tropical wave types causing rainfall modulation over northern tropical Africa: the Madden–Julian oscillation (MJO), equatorial Rossby waves (ERs), tropical disturbances (TDs, including African easterly waves), Kelvin waves, mixed Rossby–gravity waves (MRGs), and eastward inertio-gravity waves (EIGs). Reanalysis and radiosonde data were analyzed for the period 1981–2013 based on space–time filtering of outgoing longwave radiation. The identified circulation patterns are largely consistent with theory. The slow modes, MJO and ER, mainly impact precipitable water, whereas the faster TDs, Kelvin waves, and MRGs primarily modulate moisture convergence. Monsoonal inflow intensifies during wet phases of the MJO, ERs, and MRGs, associated with a northward shift of the intertropical discontinuity for MJO and ERs. This study reveals that MRGs over Africa have a distinct dynamical structure that differs significantly from AEWs. During passages of vertically tilted imbalanced wave modes, such as the MJO, TDs, Kelvin waves, and partly MRG waves, increased vertical wind shear and improved conditions for up- and downdrafts facilitate the organization of mesoscale convective systems. The balanced ERs are not tilted, and rainfall is triggered by large-scale moistening and stratiform lifting. The MJO and ERs interact with intraseasonal variations of the Indian monsoon and extratropical Rossby wave trains. The latter causes a trough over the Atlas Mountains associated with a tropical plume and rainfall over the Sahara. The presented results unveil which dynamical processes need to be modeled realistically to represent the coupling between tropical waves and rainfall in northern tropical Africa.

1. Introduction

The West African monsoon (WAM) system strongly affects livelihoods in northern tropical Africa. The highly weather-dependent agricultural sector employs 60% of the work force in West Africa and contributes 35% of the gross domestic product (GDP; Jalloh et al. 2013). As the WAM exhibits considerable variability on daily to subseasonal time scales (Janicot et al. 2011), farmers and pastoralists can substantially benefit from weather forecasts and adapt their cropping (Roudier et al. 2016) or herding strategies (Rasmussen et al. 2014). Current global numerical weather prediction (NWP) models show some skill predicting synoptic-scale weather features in this region (Elless and Torn 2018), yet they still almost entirely fail to deliver accurate and reliable rainfall forecasts (Vogel et al. 2018).

Although rainfall over northern tropical Africa is highly stochastic by nature, predictability exists on different temporal and spatial scales, as, for example, tropical waves are known to modulate precipitation. Specifically, convectively coupled equatorial waves (CCEWs) stand out against the background noise of tropical rainfall (Wheeler and Kiladis 1999). The theory of a shallow-water system yields several eigenmodes of motion that are trapped near the equator (Matsuno 1966). These waves can broadly be classified into balanced and imbalanced modes. The former are called equatorial Rossby (ER) waves, because they follow quasigeostrophy, just as Rossby waves in the midlatitudes. The

Denotes content that is immediately available upon publication as open access.

Supplemental information related to this paper is available at the Journals Online website: https://doi.org/10.1175/JCLI-D-18-0651.s1.

Corresponding author: Andreas Schlueter, andreas.schlueter@kit.edu

DOI: 10.1175/JCLI-D-18-0651.1

latter are inertio-gravity waves, which are subdivided into westward- and eastward-moving types (WIG, EIG). Additionally, two special solutions exist. Mixed Rossby–gravity (MRG) waves behave as balanced modes when traveling westward and as unbalanced waves when traveling eastward. Kelvin waves have pure gravity wave properties in zonal direction and are quasigeostrophically balanced in the meridional direction. These eigenmodes have periods of less than a day to several weeks. Each wave type is associated with specific circulation patterns. Theoretical structures of all CCEWs are displayed in Matsuno (1966, his Figs. 4–8) and Kiladis et al. (2009, their Fig. 3).

CCEWs also modulate the vertical thermodynamical structure of the tropical troposphere. Despite their different scales and circulation patterns, all CCEWs, except the equivalent barotropic ER waves (Yang and Hoskins 2017), have a self-similar, tilted vertical structure (Mapes et al. 2006; Kiladis et al. 2009). Moisture anomalies starting at low levels, rise to midlevels prior to the convective peak. A stratiform moist outflow is left behind after the passage of the deep convection. In addition to adiabatic heating associated with the vertical circulation, diabatic effects create heating that slows down the wave. The reader is referred to Kiladis et al. (2009) for a more detailed review of the theory, observational evidence, and properties of CCEWs.

Two additional disturbances dominate rainfall variability over northern tropical Africa. The Madden–Julian oscillation (MJO) is a wave mode that is not predicted by the shallow-water equations but shares several properties with Kelvin waves (Madden and Julian 1971; Roundy 2012). It is a global mode with highest activity over the Indian and Pacific Oceans. The MJO modulates the occurrence of tropical rain clusters on the intraseasonal time scale and its influence has been documented for northern tropical Africa (e.g., Matthews 2004; Pohl et al. 2009; Alaka and Maloney 2012). Different theories have been proposed to explain its existence [see reviews by Zhang (2005) and Zhang (2013)]. Tropical disturbances (TDs) are westward traveling systems off the equator with a period of 2–5 days and are often precursors of tropical storms (Riehl 1945; Roundy and Frank 2004). Over northern tropical Africa, they mostly correspond to African easterly waves (AEWs), which are a barotropic–baroclinic wave mode specific to the WAM system forming along the African easterly jet (AEJ; Reed et al. 1977; Duvel 1990). They couple to convection and dominate variability at the daily time scale (Fink and Reiner 2003; Lavaysse et al. 2006). All CCEWs, the MJO, and TDs are collectively termed ''tropical waves'' in this paper.

In the first part of this study, Schlueter et al. (2019, hereafter Part I) reviewed the modulation of rainfall by tropical waves. Depending on wave type, the modulation intensity varies from less than 2 to more than 7 mm day^{-1} during the monsoon season. Individual types can explain up to one-third of rainfall variability on the daily to subseasonal time scales. The TD and Kelvin modes control precipitation on the daily time scales. ER waves and the MJO dominate longer time scales (see Part I and the references therein).

Disturbances in the tropics are not independent from the extratropics. Using weather observations made during the Second World War, Riehl (1950) documented how tropical disturbances interact with the extratropical circulation. Predictability in the extratropics on the intraseasonal time scale largely originates from the tropics (Waliser et al. 2003; Vitart and Robertson 2018). The MJO is linked to several intraseasonal modes of variability, including the North Atlantic Oscillation (NAO) (Walker and Bliss 1932), the Arctic Oscillation (AO) (Thompson and Wallace 1998), and the Pacific–North American (PNA) pattern (Wallace and Gutzler 1981). A review of intraseasonal tropical–extratropical interactions can be found in Stan et al. (2017).

Part I showed that the MJO and ER waves over northern tropical Africa are associated with rainfall far into the subtropics during the extended monsoon season. The eastward-tilted precipitation pattern resembles tropical cloud plumes (Knippertz 2003; Knippertz et al. 2003; Knippertz and Martin 2005; Fröhlich et al. 2013). Tropical plumes are more frequent during the winter half year when troughs triggered by breaking Rossby waves draw moist monsoonal air masses deep into the subtropics. During the monsoon season, the subtropical jet (STJ) lies farther to the north and thus tropical plumes are rare then (Fröhlich et al. 2013). It is not known whether the precipitation patterns associated with ER waves and the MJO are triggered by the same dynamical process as in wintertime tropical plumes.

The influence of tropical waves on rainfall depend on their influence on the local dynamics and thermodynamics. Several studies have analyzed the (thermo) dynamic signatures of single wave types over this region in detail (e.g., TD: Reed et al. 1977; Duvel 1990; Fink and Reiner 2003; Mekonnen et al. 2006; Lavaysse et al. 2006; Janiga and Thorncroft 2016; Kelvin: Mounier et al. 2007; Nguyen and Duvel 2008; Mekonnen et al. 2008; Ventrice and Thorncroft 2013; Mekonnen and Thorncroft 2016; MJO: Matthews 2004; Janicot et al. 2009; Pohl et al. 2009; Berhane et al. 2015; Zaitchik 2017; ER: Janicot et al. 2010; Yang et al. 2018; MRG: Yang et al. 2018; Cheng et al. 2019). The comparison of results for different waves is hampered by the use of different methodologies in the respective studies. So far no systematic comparison of all tropical waves has been performed

using one consistent method. The aim of the present study is to close this gap and to provide a comprehensive analysis of the modulation of the WAM by tropical waves. This study will focus specifically on the effect of tropical waves on important components of the WAM such as the monsoon layer, intertropical discontinuity (ITD; Lélé and Lamb 2010) position, Saharan heat low (SHL; Lavaysse et al. 2009, 2010) and AEJ. Additional attention is paid to the conditions for the organization of mesoscale convective systems (MCSs; Houze 2004), which are responsible for the majority of rainfall in West Africa (Eldridge 1957; Laing et al. 1999; Fink and Reiner 2003) and commonly cause extreme precipitation (Engel et al. 2017; Lafore et al. 2017). To make use of as much data as possible in this data-scarce region, reanalysis data and in situ measurements by radiosondes will be compared. More specifically the following research questions will be addressed:

- How do circulation patterns associated with tropical waves modify the WAM and the moisture distribution?
- How do tropical waves influence the vertical profile of temperature, moisture, and wind, and what does this imply for rainfall generation and organization of MCSs?
- How is rainfall triggered over the Sahara by the MJO and ER waves and do they interact with the extratropical circulation?

In the following section the applied methods will be elaborated. The results will be presented and discussed in section 3. The summary in section 4 concludes this study.

2. Methods

a. Data

The modulation of dynamics and thermodynamics by tropical waves was examined using reanalysis data. Reanalysis products have the advantage of global coverage and a long temporal record. ERA-Interim is the most recent reanalysis product provided by the European Center for Medium-Range Weather Forecasts (ECMWF; Dee et al. 2011), until it will be fully replaced by ERA-5. Several dynamical and thermodynamical fields were downloaded from the Meteorological Archival and Retrieval System (MARS) (http://apps.ecmwf.int/datasets/). The analyzed vertically integrated fields of convective available potential energy (CAPE), moisture flux, and moisture flux convergence are computed from the surface to the top of the model domain (0.1 hPa) and were provided by the ECMWF.

The daily interpolated National Oceanic and Atmospheric Administration (NOAA) OLR dataset (Liebmann and Smith 1996) was used to filter the waves following the methods applied in Part I. OLR has the advantage that it is available for a relatively long period. Consistent with Part I, the time period spans from 1981 to 2013. The precipitation patterns associated with each wave band are discussed in detail in Part I. As in Part I, the Climate Hazards Group Infrared Precipitation with Station data, version 2 (CHIRPS), dataset was used to visualize the associated rainfall anomaly patterns. CHIRPS estimates daily precipitation rates over landmasses only by gauge calibration of infrared measurements and has a spatial resolution of 0.25° × 0.25° (Funk et al. 2015).

Reanalyses have large biases in humidity fields but also in wind and temperature over the measurement-sparse African continent (Agustí-Panareda et al. 2010a,b; Roberts et al. 2015). Thus, in situ measurements by radiosondes are a valuable supplement to accurately assess the modulation of atmospheric profiles. For this purpose, quality-controlled radiosonde measurements from the Integrated Global Radiosonde Archive (IGRA), version 2 (Durre et al. 2016), were analyzed (downloaded from https://data.nodc.noaa.gov/cgi-bin/iso?id=gov.noaa.ncdc:C00975). Because of a relatively high data availability, 1200 UTC ascents at Abidjan Airport (13.48°N, 2.17°E, Abidjan, Ivory Coast) and Niamey Airport (5.25°N, 3.93°W, Niamey, Niger) were chosen to illustrate the modulation over the Guinea Coast box (5°W–5°E, 5°–10°N) and the West Sahel box (5°W–5°E, 10°–15°N) defined in Part I. Composites of radiosonde ascents from Abidjan were calculated for the more equatorial MRG and Kelvin waves, as both are predominantly equatorial phenomena, whereas the influence of ER waves and TDs was analyzed using the Niamey data, as both wave modes have a stronger imprint farther to the north (see Part I, their Figs. 4–6). Between April and October 1981–2013, 1370 measurements are available for Niamey (19.4% of the study period) and 1214 measurements (17.2%) for Abidjan. As reference for the observed rainfall, the daily rain gauge observations were obtained from the Karlsruhe African Surface Station Database (KASS-D).

The influence of the MJO was compared with the NAO, AO, and PNA. (Daily normalized indices for these modes were downloaded from ftp://ftp.cpc.ncep.noaa.gov/cwlinks. Further information on how the indices are calculated can be found at http://www.cpc.ncep.noaa.gov/products/precip/CWlink/daily_ao_index/history/method.shtml.

b. Wave filtering

The same approach as in Part I was applied to identify tropical waves. In a nutshell, OLR was filtered using the classical method by Wheeler and Kiladis (1999). The same filtering bands for the six waves MJO, ER, TD, Kelvin, MRG, and EIG were applied (Table 1 in Part I).

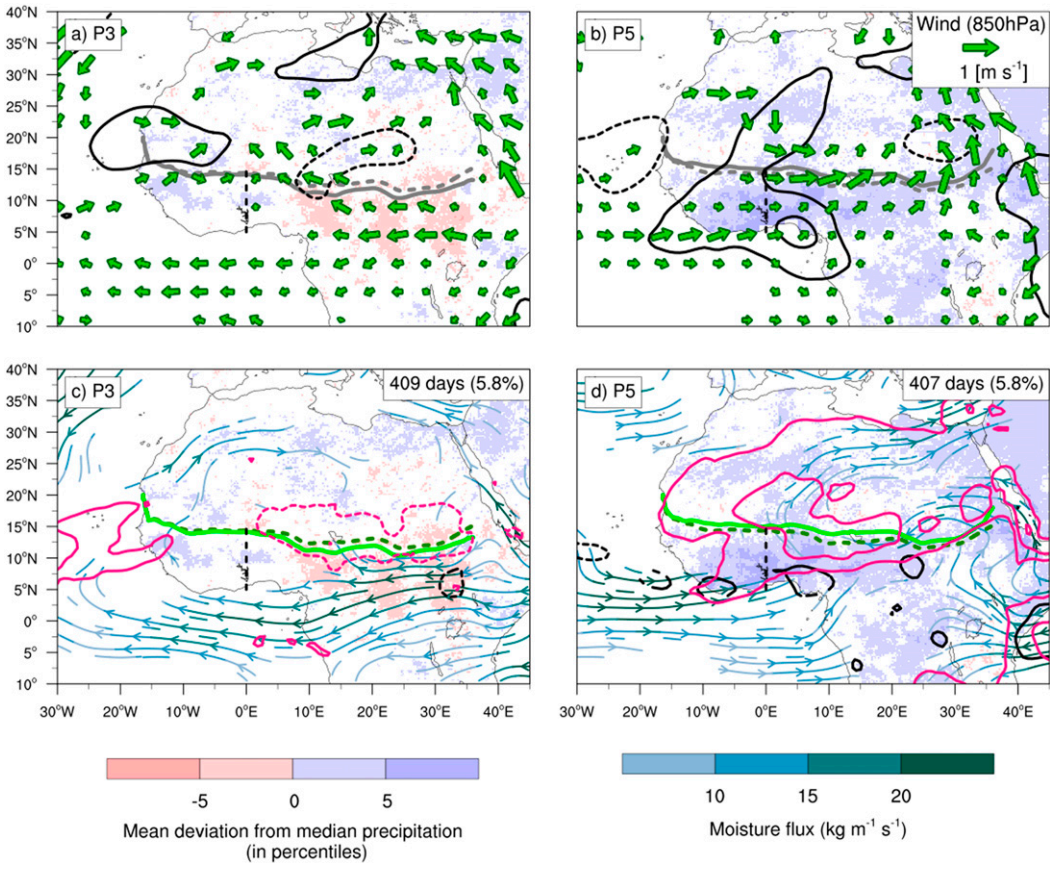

FIG. 1. Composites of days with significant Madden–Julian oscillation signal in (left) phase 3 (neutral phase) and (right) phase 5 (wet phase) over 5°–15°N, 0°E (dashed vertical line) during the extended monsoon season (March–October). (a),(b) Composites of significant anomalies of 850-hPa wind (green arrows) and divergence at 200 hPa (thick contours from -3×10^{-6} to 3×10^{-6} s^{-1} in steps of 0.5×10^{-6} s^{-1}; convergence dashed). (c),(d) Significant anomalies of moisture flux (streamlines; magnitude in turquoise colors), moisture flux convergence (black lines; at ± 1 and 2×10^{-5} kg m^{-2} s^{-1}; divergence dashed), and PW (pink lines, at ± 1, 2, and 3 mm; negative dashed). Significant precipitation anomalies are shaded (see Part I, their Figs. 5 and 6). The mean position of the ITD in each phase is depicted with a gray line in (a) and (b) and a green line in (c) and (d). The dashed gray line in (a) and (b) and dark green line in (c) and (d) show the mean ITD position in all phases. The number of days and the fraction of days per season during each phase are indicated in the top-right corner of (c) and (d).

No symmetric/antisymmetric decomposition about the equator was imposed. Background noise also projects into the filter bands (Wheeler and Kiladis 1999), but this is likely removed when compositing over many cases as done here. It should be noted that filtered signals are related to convectively coupled waves and not to dry equatorial waves because low OLR indicates convective activity. Thus, conclusions cannot be readily transferred to the impact of dry equatorial waves on the WAM system.

c. *Composite study*

A local wave phase metric was constructed based on the wave signal at 0°E and its time derivative (Riley et al. 2011; Yasunaga and Mapes 2012). The phase–amplitude space was divided into eight phases, excluding days when the amplitude is not significant. The reader is referred to Part I for further details of the method.

Composites of several dynamic and thermodynamic fields were calculated for all days when the respective wave is in each phase (Figs. 1–5). Lower-tropospheric wind and upper-level divergence fields are used to portray the dynamic structure. The moisture transport is analyzed using anomalies of moisture flux, moisture flux convergence, precipitable water (PW), and CHIRPS precipitation during all phases. A spatial smoothing of 2° and 5°, respectively, was applied to wind and moisture flux divergence fields. The position of the ITD gives an estimate of the northward extent of the monsoon layer. The ITD is commonly indicated by the isoline of 14°C

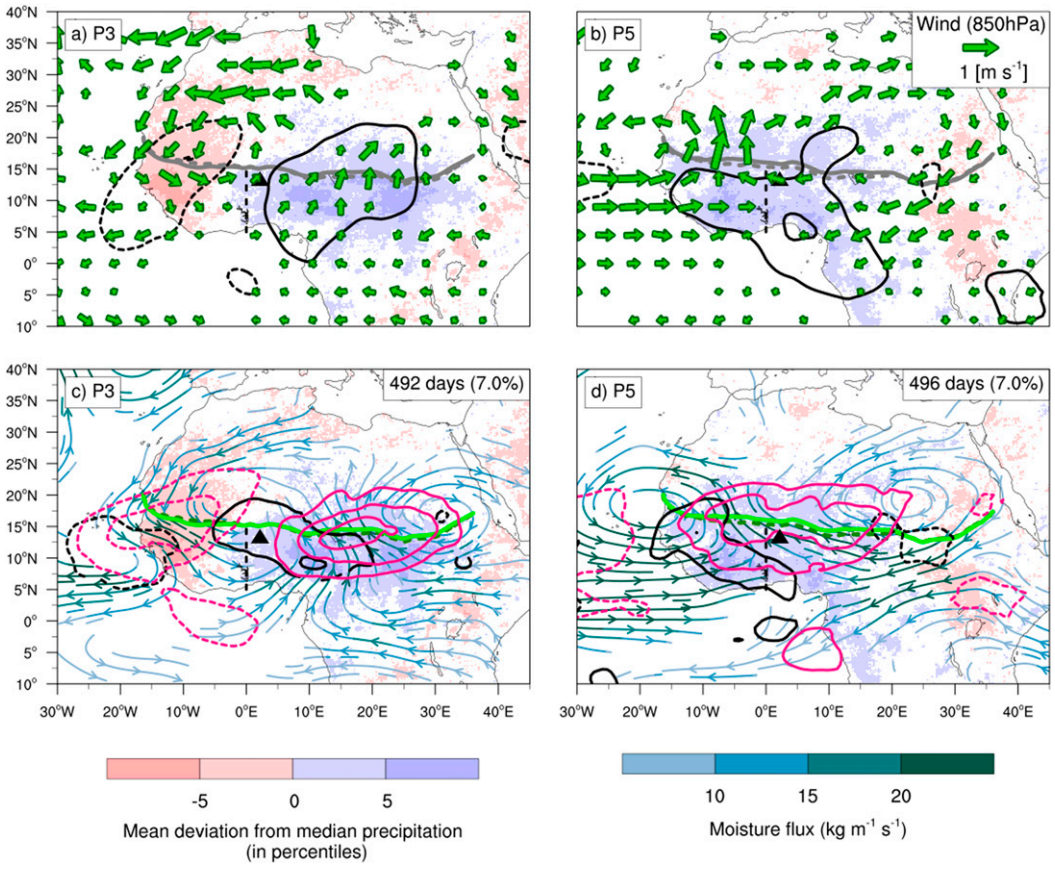

FIG. 2. As in Fig. 1, but for equatorial Rossby waves. The triangle shows the location of the radiosonde station in Niamey used in Fig. 7a.

dewpoint temperature at 2 m (Buckle 1996). Exemplarily, plots of the waves in a neutral and wet phase are presented (Figs. 1–5). Composites of all eight phases can be found in the online supplemental material (Figs. S1–S12).

The influence of tropical waves on the organization of MCSs was analyzed using three variables that are known to be key ingredients for MCSs (Nicholls and Mohr 2010; Maranan et al. 2018). CAPE is a general measure for atmospheric instability and the strength of convective updrafts (Moncrieff and Miller 1976). Second, dry midlevels intensify evaporative downdrafts in MCSs (Raymond and Jiang 1990; Brown and Zhang 1997). These downdrafts induce cold pools, which reinforce the MCS (Zipser 1977; Corfidi 2003). The strength of downdrafts was estimated using relative humidity at 500 hPa (RH_{500}) following Roca et al. (2005). Finally, low-level wind shear is necessary for MCSs to separate up- and downdrafts and support the longevity of the system (Browning and Ludlam 1962; Rotunno et al. 1988). Here, we use the total wind difference between 600 and 925 hPa ($Shear_{600–925}$). Mean CAPE, RH_{500}, and $Shear_{600–925}$ anomalies were calculated for each phase in the Guinea Coast and West Sahel boxes.

Mean anomalies of all fields were calculated with respect to the climatology from 1979 to 2016. (Significance in Figs. 1–6 and 10 was tested at the 5% level using nonparametric bootstrapping and $n = 1000$ repetitions.) Wind anomalies are considered significant when either the zonal or meridional anomaly was significantly different from zero.

d. Radiosonde study

Most radiosonde ascents lack measurements above 300 hPa, and thus only RH below 300 hPa was analyzed. The raw data were read with the Python package IGRA2reader and interpolated to every 5 hPa, and then composites of all ascents during all eight wave phases were constructed. To capture the local wave signal over the station, the wave phases were determined for a narrower Guinean and Sahelian zonal wave band. In Abidjan, wave phases were calculated based on 5°–10°N, 4°W, in Niamey based on 10°–15°N, 2°E. The absolute difference of the wind vector at 600 and 925 hPa was calculated for each profile and averaged for each phase.

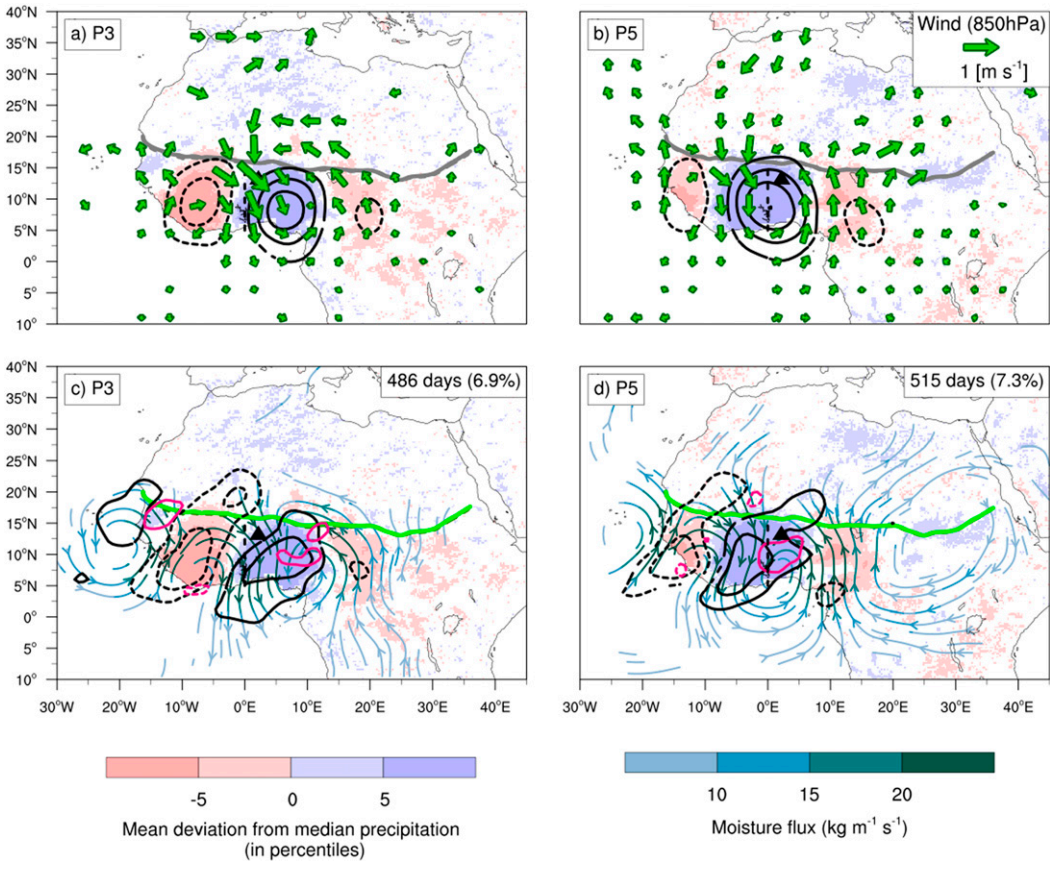

FIG. 3. As in Fig. 1, but for tropical depressions (AEWs). The triangle shows the location of the radiosonde station in Niamey used in Fig. 7a.

To analyze the thermodynamic conditions during the passage of the waves, mixed layer parcel buoyancy of the mean profile during all phases was calculated following Schrage et al. (2006). The parcel buoyancy at a pressure level with the environmental temperature T_e is defined as

$$B = T_p - T_e,$$

where T_p is the parcel profile ascending dry adiabatically until the lifting condensation level and moist adiabatically above this level. The parcel profile was determined based on the mean temperature and humidity of the mixed layer between 15 and 65 hPa above ground (approximately 400 m). The lowest 10 hPa were removed before the parcel profile was calculated because of contamination from inconsistent surface measurements that stem from radiosonde initialization. Parcel buoyancy can be used to analyze the vertical stability. By definition $B = 0$ at the level of free convection (LFC) and at the equilibrium level (EL). The integral of B between the surface and LFC is proportional to CIN, and the area between the LFC and EL to CAPE.

The rainfall signal was plotted using rain gauge data from the stations, where the radiosondes were launched. Rain gauges report daily rainfall from 0600 to 0600 UTC + 1 day, whereas radiosonde are launched at 1200 UTC. The shift of six hours was eliminated using the method we presented in Part I: The mean periods of the respective waves were calculated using MATLAB function meanfreq(). Based on this, the length of six hours measured in wave phases was estimated in order to shift the precipitation curve to match the radiosonde data.

e. *Time-lagged analysis*

The MJO and ER waves trigger rainfall anomalies up to the Mediterranean Sea (Part I). To test, whether and how the waves couple with the extratropical circulation, geopotential and wind at 300 hPa were analyzed. The influence on lower-tropospheric thickness was analyzed between 600 and 925 hPa. The origin and development of the wave signal were traced using a time-lag analysis. The tropical plumes were observed in the local phase 4 (see section 2d of Part I for more detail on the phase diagram) for the MJO and in phase 6 for ER waves.

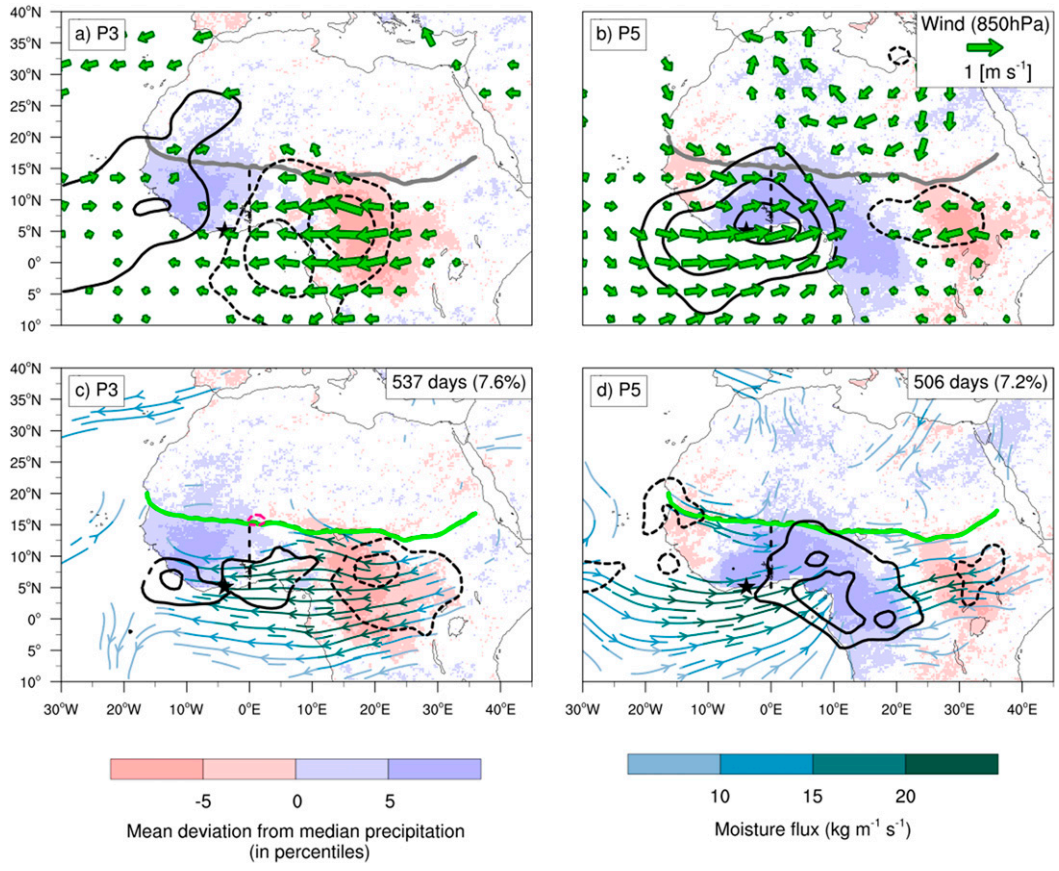

FIG. 4. As in Fig. 1, but for Kelvin waves. The star shows the location of the radiosonde station in Abidjan used in Fig. 7c.

Composites of significant anomalies of precipitation, geopotential, and wind in 300 hPa were calculated for 25–5 days after the MJO wave was in phase 4 and 15–3 days after the ER was in phase 6.

3. Results

This section will describe first the circulation patterns of the different wave types and their influence on the moisture distribution. Then, their vertical structure will be examined and differences in mechanisms of rainfall modulation will be shown. The last part of this section will analyze how rainfall over the Sahara is triggered by the MJO and ER waves and discuss how these waves interact with the extratropical circulation during such rainfall events.

a. Circulation patterns and moisture modulation

The MJO strongly modulates zonal winds and features vortices off the equator (Figs. 1, S1, and S7). Hence, it shares dynamical properties of Kelvin waves, also impacting zonal winds, and ER waves with their off-equatorial vortices (Matsuno 1966). This is consistent with the suggestion that the MJO over Africa is a result of Kelvin and Rossby wave responses to enhanced convection over the warm pool (Matthews 2004; Janicot et al. 2009; Alaka and Maloney 2012). Matching results over oceanic regions (Wheeler and Hendon 2004), the wet phase over northern tropical Africa lies in a region of enhanced westerlies. The observed MJO pattern over Africa has a more standing component (see Fig. S1 and Pohl et al. 2009). Upper-level divergence and weak low-level convergence are associated with lifting of air parcels and thus moistening of the air and increased precipitation (Figs. 1b,d). The MJO has a large-scale influence on PW (Fig. 1d) as shown previously (Matthews 2004; Alaka and Maloney 2012). Lavender and Matthews (2009) argue though that the increased boundary layer moisture is rather a result of enhanced convection than a cause, which is consistent with the lag between precipitation and PW observed in Fig. S7. The monsoonal flow intensifies during wet phases and reduces during dry phases. In central and eastern Africa, the ITD moves southward

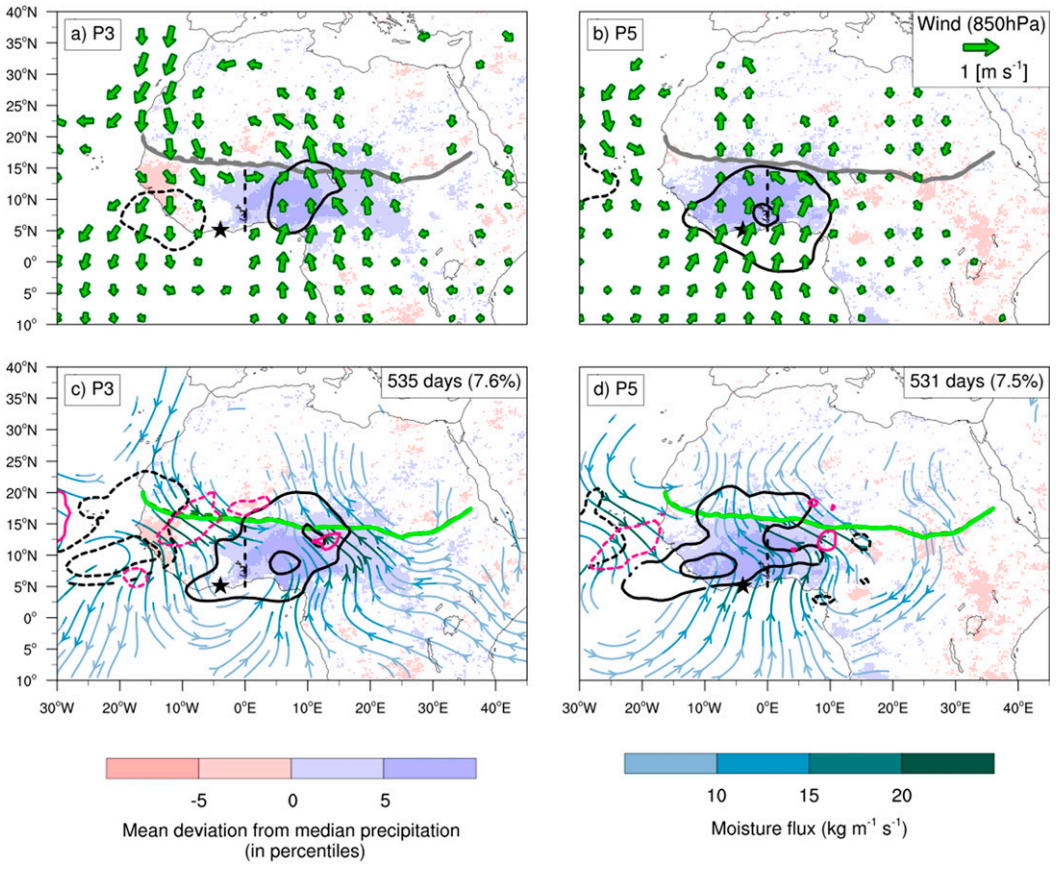

FIG. 5. As in Fig. 1, but for mixed Rossby–gravity waves. The star shows the location of the radiosonde station in Abidjan used in Fig. 7b.

by 100–200 km during the dry phases and northward during the wet phases (Figs. 1d and S1). West of 5°E, the modulation of the ITD is weaker. The SHL is ventilated by monsoonal and Atlantic air masses. Significant moisture anomalies can be found far into the subtropics (>30°N). The relationship with the extratropics will be discussed in section 3c. Because of the low frequency of the MJO, the total moisture convergence is small compared to the other wave types. As a side remark, the enhanced westerlies during the wet phase lead to increased cyclonic shear vorticity at the southern flank of the AEJ (Matthews 2004; Ventrice et al. 2011). This affects the stability of the AEJ and thus the AEW occurrence is modified (Alaka and Maloney 2012, 2014).

The more rotational ER waves show westward-propagating vortices with centers off the equator at around 20°N (Figs. 2, S2, and S8). Sustained moderate moisture convergence during the passage of the slow-moving ER waves result in a strong modulation of PW and precipitation is mainly aligned with these anomalies. Moist air masses from the Gulf of Guinea and Congo basin are transported toward tropical West and central Africa during the wet phase. In the Sahel, wet conditions are related to enhanced monsoonal flow and dry conditions with decreased monsoonal inflow. The mean position of the ITD is roughly 100 km farther north in the wet sector of the wave and farther south in the dry sector. The SHL is ventilated by southerlies during phases 5–7 (Figs. 2d and S2). These southerlies result in moisture and precipitation anomalies reaching up to the Mediterranean. As discussed in the first part of this study, a tropical-plume-like rainfall pattern is observed over the Sahara during phase 6 (Fig. S8f). The triggering of this plume and the relationship to the extratropics will be discussed in section 3c. The circulation patterns presented here are comparable with results in previous studies (Janicot et al. 2010; Thiawa et al. 2017). It should be noted that ER waves are likely related to the so-called Sahel mode of intraseasonal rainfall variability (Sultan et al. 2003; Janicot et al. 2010).

TDs have a strong influence on the upper-level divergence field (Figs. 3a,b and S5) because of their strong coupling with convection. The flow is modulated up to roughly 25°N. TDs correspond mainly to AEWs over

Africa (Roundy and Frank 2004). Thus, the circulation patterns of TDs presented here match well with the typical structure of AEWs. In the trough of the AEW and ahead of it in the region of northerlies, precipitation is enhanced (Duvel 1990; Fink and Reiner 2003; Janiga and Thorncroft 2016). A secondary maximum, which can be found in the region of southerlies, is not resolved by the filtering method applied here. It should be noted that the position of precipitation and dynamical forcing has been described to change substantially when the wave moves offshore (Kiladis et al. 2006), which is not visible in Fig. 3. The vortices related to the modulation of the AEJ, result in moisture flux convergence and divergence (Figs. 3c,d and S11). The zonal gradient of moisture at the boundary of the monsoon layer (not shown) leads to a tilt of the moisture flux convergence fields. This tilt can also be seen in composites of TRMM precipitation (Part I, their Fig. S11). In the wake of the precipitation maxima and minima, PW is slightly reduced and enhanced, respectively. Associated with the northerlies in the dry sector and southerlies in the wet sector, the mean position of the ITD modulates by about 50–100 km. A weak cross-equatorial flow might stem from contamination by MRG waves, which have a partial overlap in the filter bands with TDs (see Part I and Cheng et al. 2019).

Kelvin waves show a pronounced influence on the zonal flow patterns symmetric about the equator (Figs. 4, S4, and S10) as predicted by theory (Matsuno 1966). Although the flow pattern is primarily zonal, an enhanced southerly component is evident in the wet phase (Fig. 4b) and a northerly component in the dry phase over West Africa (Fig. S4a). Theoretical studies predict this additional meridional circulation, if the forcing lies off the equator (Gill 1980; Dias and Pauluis 2009). The observed circulation patterns are consistent with previous studies over Africa (Mounier et al. 2007; Mekonnen et al. 2008; Nguyen and Duvel 2008; Sinclaire et al. 2015; Thiawa et al. 2017). The wet phases are associated with regions of enhanced low-level westerlies and vice versa. This deviates from dry inviscid linear theory that would predict precipitation in quadrature with the zonal wind. As convectively coupled Kelvin waves are vertically tilted, the lower-level convergence center leads the precipitation anomalies, with upper-level divergence lagging by approximately 1/8 of the wavelength (cf. top panels of Fig. 4 with bottom panels). The vertical structure will be discussed in detail in the following subsection. Similar to the MJO, westerlies during the wet phase lead to increased horizontal shear on the southern flank of the AEJ. Kelvin waves facilitate precipitation mainly because of moisture flux convergence (Fig. 4d). Because moisture has a low gradient meridionally (not shown), the moisture flux convergence is predominantly generated via convergence of zonal winds. The mean ITD position does not shift significantly. The influence on precipitation and circulation reaches into the Sahel to about 15°N. As Kelvin waves quickly move over Africa and moisture is removed by precipitation, PW is not strongly affected.

MRG waves over the African continent are not well studied. They are a more rotational wave type and feature deep westward-moving vortices reaching from 850 to 300 hPa and centered at around 25°–30°N (Figs. 5, S3, and S9). Consistent with shallow-water theory, they modulate the cross-equatorial meridional flow. Precipitation is mainly related to moisture flux convergence. Similar to the faster-moving TDs and Kelvin waves, the modulation of PW is weaker compared with the MJO and ER waves. As MRG waves have a strong meridional component at the equator, moist air masses are transported northward originating from the Gulf of Guinea and Congo basin. These moisture anomalies reach up to 20°N. The mean ITD position, however, is not significantly affected. Moisture flux convergence directly at the Guinea Coast leads the anomalies farther inland. In the subtropics, a westward-propagating signal can be observed at 300 hPa (Fig. S3). MRG waves share several similarities with TDs. As their spectral bands partially overlap, both modes can project onto each other. Over the Pacific, MRG waves can transition to off-equatorial TDs (Takayabu and Nitta 1993). Both wave modes closely interact over Africa (Yang et al. 2018). Despite the spectral overlap, the clearly different circulation patterns of MRGs (Fig. 5) and TDs (Fig. 3) indicate that MRG waves are in fact a distinct wave mode over Africa and should be treated individually. The most notable difference is that enhanced precipitation in MRG waves is found in the low-level southerlies, whereas TDs feature enhanced precipitation in the region of northerlies.

The influence of EIG waves on the circulation and moisture fields is weak and, thus, the corresponding plots are only shown in the supplementary material (Figs. S6 and S12). As predicted by shallow-water theory, regions of upper-level divergence and positive precipitation anomalies in the Northern Hemisphere are related with northerlies, and vice versa (Figs. S6a,d). The moisture distribution and ITD position are hardly influenced. The role of EIG waves on the WAM has not been studied so far. This study shows that the influence of EIG waves on the dynamics and thermodynamics of the WAM is minor. EIG waves are more difficult to capture because of their weak influence on circulation (Kiladis et al. 2016). A drawback of the applied methods is that the filtering, which is based on daily OLR measurements, might miss the subdaily EIG

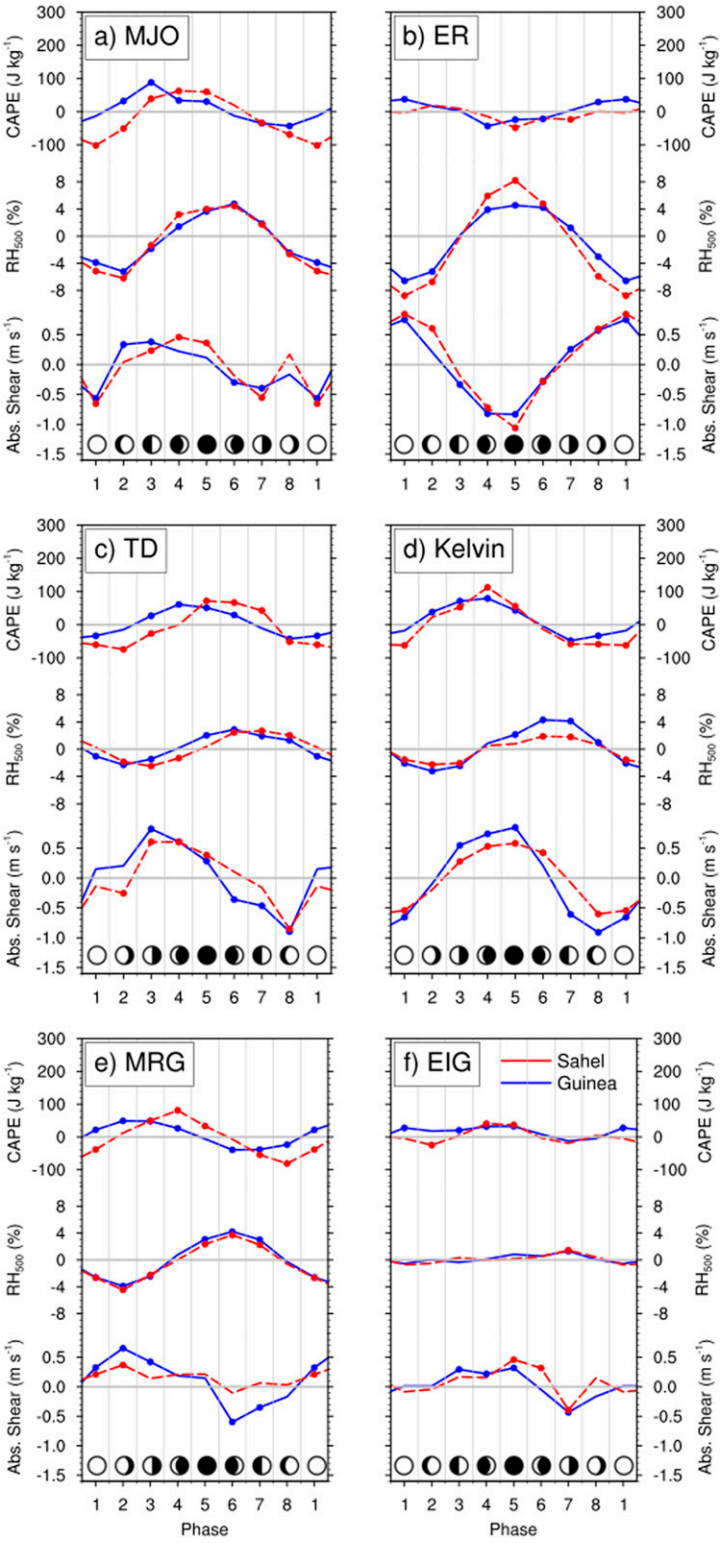

FIG. 6. (a)–(f) Modulation of CAPE, RH_{500}, and the low-level wind shear between 600 and 925 hPa in the Sahel box (dashed red line) and Guinea box (solid blue line) during all 8 phases for six tropical waves. Significant anomalies are marked with a solid circle. Small moon symbols indicate the phase of the wave, with dry anomalies in white and wet anomalies in black (see Figs. S1–S12).

signal. Additionally, reanalysis might not adequately capture these imbalanced modes, which are to a large extent not assimilated by current NWP models (Žagar et al. 2016).

b. *Vertical structure and mechanism of rainfall modulation*

The mechanisms of rainfall modulation depend on the vertical profile of the tropical waves. Figure 6 shows the modulation of three key ingredients for MCS organization in two boxes in West Africa as measured by reanalysis data. To give a more detailed picture of the vertical structure of ER waves, TDs, Kelvin waves, and MRG waves, radiosonde data are also analyzed (Fig. 7). No consistent modulation of radiosonde data was found for the MJO and EIG waves and, thus, their composites are not shown here.

The MJO indicates facilitated conditions for organization of MCSs in the reanalysis data. CAPE in the Guinea Coast leads the convective maximum by two phases and is in phase with convection in the West Sahel (Fig. 6a). Before the wet peak, absolute wind shear increases and decreases sharply after the peak. Convective downdrafts are likely weaker during wet phases, as midlevel moisture is enhanced. Conditions for MCSs are favorable before and during the wet peak of rainfall and slightly unfavorable after the peak in rainfall.

ER waves (Fig. 6b) demonstrate a unique modulation of thermodynamic conditions with unfavorable conditions for MCSs during the wet phases. In contrast to the other wave types, CAPE and wind shear are reduced during wet phases and enhanced during dry phases, although the CAPE anomaly is weak. Midlevel moisture is strongly enhanced during the wet phases of ER waves and decreased during dry phases. Radiosonde data at Niamey give a more detailed view on the vertical structure of ER waves (Fig. 7a). In contrast to the following waves, ER waves are not tilted vertically and suggest instead a deep barotropic structure. During the passage of ER waves, the entire troposphere moistens and then dries. In the midtroposphere, absolute RH increases and decreases by more than 10%. Consistent with reanalysis data, the effect on parcel buoyancy is weak. LFC and CIN are slightly lowered during the wet phase. Winds turn cyclonically with time consistent with Fig. S2. The AEJ is weaker before the wet phase and stronger afterward. Upper-level wind divergence leads the rainfall maximum. This indicates that precipitation is mainly generated by large-scale lifting and moistening.

The influence of TDs (Fig. 6c) on organization of convection resembles the modulation by Kelvin waves. The phasing and magnitude of CAPE, midlevel moisture, and wind shear anomalies are remarkably similar. Wind shear anomalies, however, are slightly weaker and do not change as abruptly compared to Kelvin waves. TDs are also tilted vertically, as the profile over Niamey shows (Fig. 7b). A very shallow region of positive humidity anomalies exists at 900 hPa during the dry phase. During phases 3–4, the troposphere moistens relatively rapidly, starting from the lower and the upper troposphere. By phase 5, the entire troposphere is moistened. Moist anomalies remain at 500–350 hPa after the passage of rain. Parcel buoyancy is strongly modulated with CAPE notably enhanced and CIN reduced before the wet peak, which is quickly diminished and increased, respectively, when deep convection occurs. After the peak of rainfall, the LFC is lifted and the EL is lowered. Consistent westerly (easterly) anomalies are evident in the lower troposphere during the dry (wet) phase. The AEJ is modulated and turns anticyclonically with time, whereas upper-level winds turn cyclonically. Wind shear increases before and during the rainfall peak. It can be concluded that rainfall is embedded in an environment that facilitates the formation of MCSs.

Kelvin waves (Fig. 6d) have similar modulation signatures as the MJO but on a shorter time scale. CAPE leads precipitation by about one phase. Midlevel moisture is reduced prior to the peak of rainfall and enhanced after the peak of rainfall. As Kelvin waves modulate zonal winds (Figs. 4 and S4), low-level wind shear is strongly modulated, which leads the wet peak by half a phase. The radiosonde measurements at Abidjan reveal a vertical tilt (Fig. 7c). Moisture anomalies build up at 900–800 hPa three phases before the peak in rainfall, rise, and finally the entire troposphere is moistened after the peak of rainfall. Upper- and midlevel moisture anomalies persist after the wet peak, while lower levels start to dry again (phases 7–8). Parcel buoyancy is strongly modulated. CAPE is enhanced before the peak of rainfall and reduces with the onset of rain. During the deep convection, CIN increases, the LFC shifts upward, and the EL is lowered. The vertical tilt of the Kelvin wave is also evident in zonal wind anomalies, which move upward with time. Meridional winds are only weakly modulated. Low-level wind shear is enhanced during the wet phase. The AEJ is strengthened during and after the dry phase, and reduces after the peak of rainfall. Upper-level winds are strongly modulated. The tropical easterly jet is enhanced during phases 5–7 and weakened during phases 8–2. Upper-level winds diverge during the peak of rainfall facilitating deep convection. In summary, the radiosonde data suggest a buildup of low-level clouds before the rainfall peak, followed by deep and well organized convection, and finally a stratiform outflow region.

The influence of MRG waves (Fig. 6e) on the thermodynamic environment is in between the MJO and ER

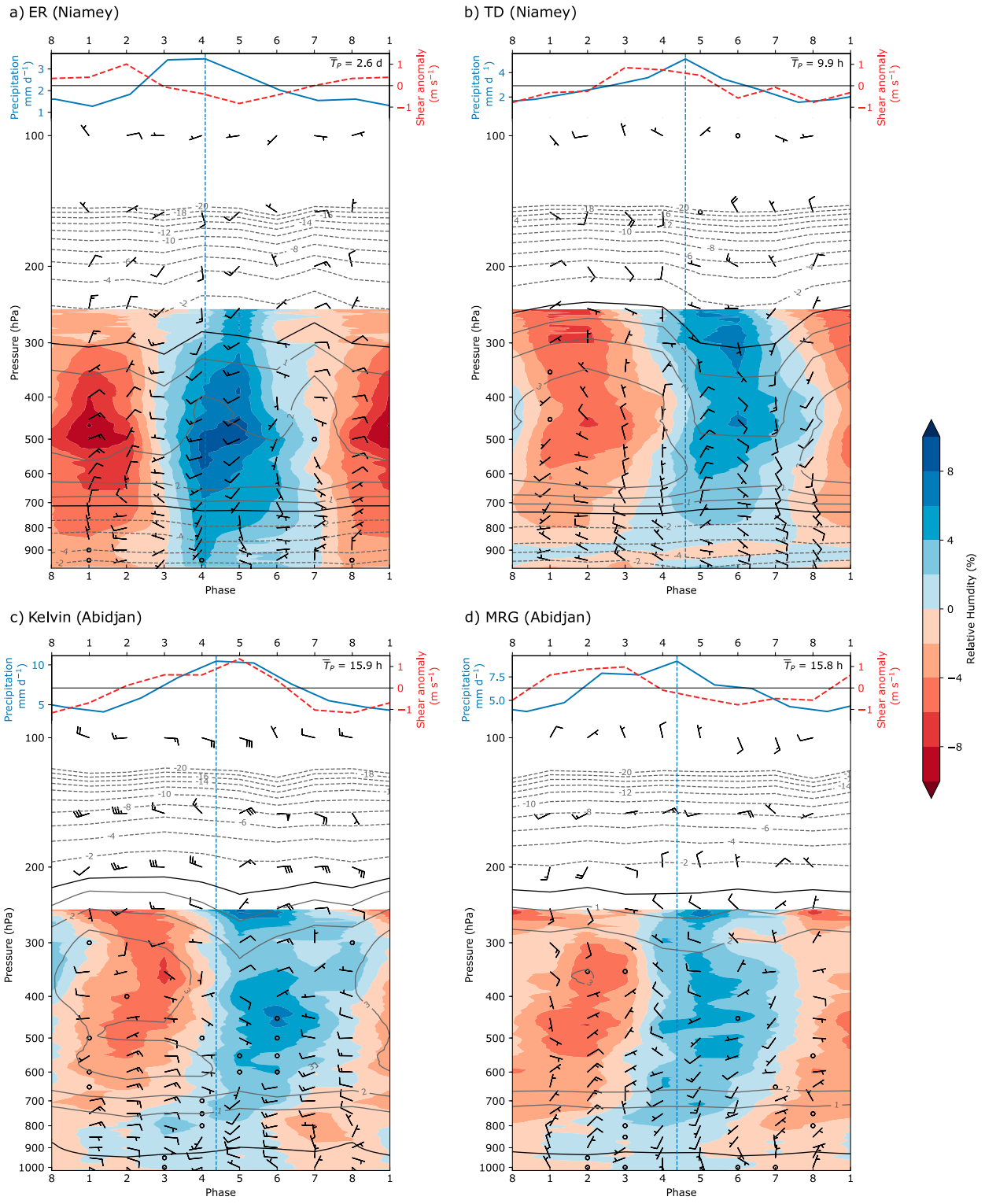

FIG. 7. Radiosonde composite for all phases of (a) ER waves and (b) TDs over Niamey, as well as (c) Kelvin and (d) MRG waves over Abidjan during April–October. Filtering was done at 2°E and 10°–15°N for Niamey and at 2°E and 5°–10°N for Abidjan. The top of each panel shows the absolute wind shear anomaly between 600 and 925 hPa (red dashed line) and precipitation anomaly (blue line) as recorded by the rain gauge at the respective location. The precipitation is shifted by 6h to account for the time difference between radiosonde and rain gauge measurement (converted by average phase length $\overline{T}_P$, see method section 2d for more detail). The blue dashed vertical line indicates the peak of rainfall. The bottom of each panel shows the relative humidity anomaly (shading), parcel buoyancy anomaly (contours; negative dashed), and horizontal wind anomaly (wind barbs; half barbs are equal to 0.5 m s^{-1}, full barbs to 1 m s^{-1}, and triangles to 5 m s^{-1}). The bottom thick black contour line represents the LFC and the top thick line the EL.

waves. CAPE anomalies lead precipitation anomalies by three phases in the Guinea Coast and by one phase in the West Sahel. Midlevel moisture is enhanced after the peak of the wet phase and suppressed after the dry phase. Wind shear anomalies lead precipitation anomalies by about two phases with a weaker modulation in the West Sahel. Radiosonde ascents at Abidjan reveal a vertical tilt (Fig. 7d). Moisture builds up at low levels (900–800 hPa) two to three phases before the peak in rainfall. The moisture anomaly shifts upward and, eventually, the entire troposphere is moistened during the rainfall peak. Upper- and midlevel moisture anomalies persist after the wet peak, while dry anomalies build up at lower levels (phases 5–7). MRG waves only weakly modulate parcel buoyancy with enhanced CAPE before the buildup of deep convection and reduced CAPE during it. The AEJ is stronger during the dry phase and weakened during the wet phase. Upper-level winds converge before the wet peak and diverge after the wet peak indicating that deep convection is first suppressed but then emerges during the wet peak. As low-level wind shear is enhanced before the wet peak and reduces after the rainfall peak, good conditions for MCS organization persist only during the wet peak. The buildup of rainfall by MRG waves is gradual over Abidjan until deep convection develops followed by a stratiform outflow region (Fig. 7d).

EIG waves (Fig. 6f) only weakly modulate CAPE, midlevel moisture, and wind shear. Wind shear is weakly enhanced before and during, and reduced after the wet phase. This study suggests that EIG waves have at most a minor influence on mesoscale organization of precipitation.

All tropical waves, except ER waves, have a similar vertical structure although they act on different time scales (Mapes et al. 2006; Kiladis et al. 2009). CCEWs are tilted vertically. Ahead of the region of enhanced rainfall, winds converge and moisture is increased at low levels. Midlevels moisten during the progression of the wave until the entire troposphere is moist during the deep convective phase. Furthermore, the Boussinesq model theoretically predicts such a behavior for imbalanced waves (Roundy and Janiga 2012). This model is an alternative theory to the shallow-water model, which additionally takes buoyancy into account. In balanced waves, buoyancy does not act as a restoring force, and thus they do not possess such a vertical tilt. The radiosonde analysis are consistent with these results. The more imbalanced modes (TDs, Kelvin waves, and partially the MRG waves) show a tilted vertical structure, whereas the balanced, equivalent barotropic ER wave lacks such a tilt (Kiladis and Wheeler 1995; Yang and Hoskins 2017; Yang et al. 2018). The tilt of ER waves depends on longitude. As the waves grow baroclinically, their tilt decreases when moving over Africa toward the Atlantic Ocean (Yang et al. 2018). To test this was beyond the scope of this study. The vertical structure of the MJO, which was not analyzed in this study, is similar to that of a Kelvin wave (Mapes et al. 2006; Tian et al. 2006; Roundy 2012; Jiang et al. 2015).

Rainfall anomalies in the more balanced ER wave are mostly related to large-scale moistening and quasigeostrophic lifting. Stratiform rain is thus facilitated. The rainfall anomaly in predominantly imbalanced waves (MJO, Kelvin, and partially MRG) is of convective nature. Increased CAPE and low-level shear as well as decreased midlevel humidity favor vigorous and organized convection during the wet phase. TDs show the same effects. As MRGs have imbalanced characteristics at low wavenumbers and transition to a quasigeostrophic behavior at higher wavenumbers (Delayen and Yano 2008), the organization of MCSs is not as strongly modulated, compared with the MJO, TDs, and Kelvin waves. Several studies have documented that favorable conditions for MCSs exist over Africa during the passage of AEWs (e.g., Duvel 1990; Fink and Reiner 2003; Janiga and Thorncroft 2016; Maranan et al. 2018) and Kelvin waves (e.g., Mounier et al. 2007; Nguyen and Duvel 2008; Laing et al. 2011; Sinclaire et al. 2015). MRG waves are also known to modulate MCSs (Holder et al. 2008). Although EIG waves are by nature imbalanced modes, this study could only reveal a minor influence on vertical profiles. Yet, it could be speculated that either the applied methods could not measure this adequately because of the high speed of EIG waves, or they are too fast to affect the time scale of convective organization.

c. *Relationship to extratropical Rossby waves*

The MJO and ER waves can trigger tropical plume-like precipitation anomalies over the Sahara. These structures appear during the local phase 4 of the MJO (Fig. S7d) and phase 6 of ER (Fig. S8f). Between April and July, 73% of cases with MJO in phase 4 occur and 74% of cases with ER in phase 6 (Fig. 8). The preference of tropical plumes during spring is even more evident when only looking at strong cases in phase 4 and 6, respectively, where the local wave amplitude is greater than 2. Of the 97 strong MJO cases, 90% occur during the extended monsoon season, and 76% of the 106 strong ER cases take place during April and May (not shown). During the premonsoon, when most of the cases happen, extratropical Rossby wave trains can penetrate far south. The breaking of these Rossby waves leads to a tilted trough near the Atlas Mountains and subsequently triggers a tropical plume (Knippertz 2003; Knippertz and Martin 2005; Fröhlich et al. 2013).

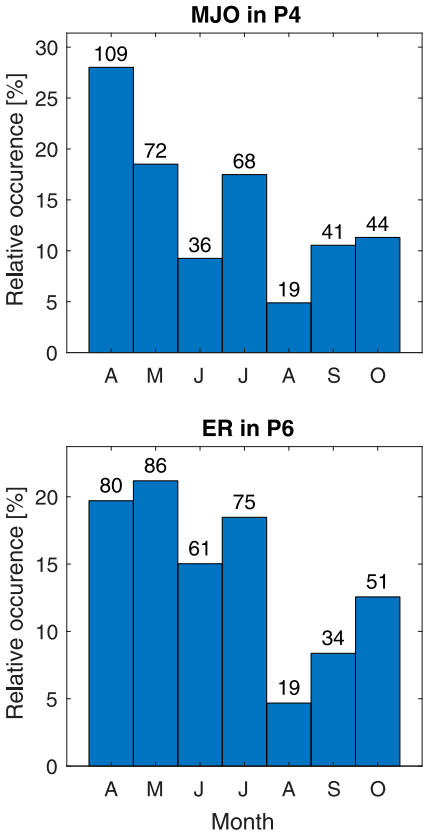

FIG. 8. Relative occurrence of months during which local (a) MJO is significant in phase 4 and (b) ER in phase 6 at 0°E. Numbers over the bars show total count of days during each month.

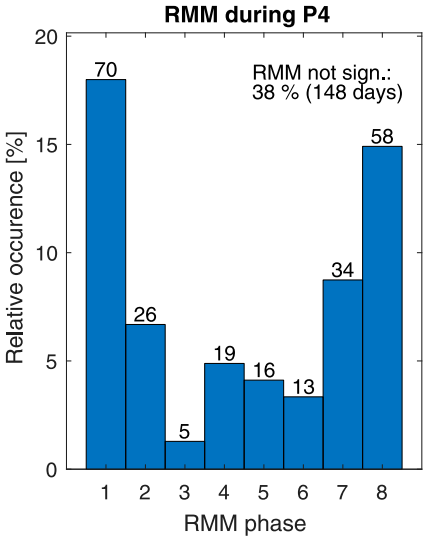

FIG. 9. RMM when local MJO is significant in phase 4. The histogram depicts the relative occurrence in each phase. Numbers over the bars show total count of days during each RMM phase. The index was obtained from http://www.bom.gov.au/climate/mjo/.

This study uses a local wave filtering. This way the local ''flavor'' of the MJO is captured more adequately. To allow comparison with the widely used real-time multivariate MJO index (RMM; Wheeler and Hendon 2004), Fig. 9 shows the RMM during the local phase 4, when the plume is observed. The MJO as a global mode is over the western hemisphere and Africa (RMM phases 1 and 8). It has to be noted also that the observed MJO pattern over Africa has a more standing component (see Fig. 10 and Pohl et al. 2009). Roughly 40% of significant local MJO events over Africa are missed by the global RMM index (Fig. 9). Thus, a direct comparison with global MJO studies is limited.

The MJO couples with extratropical Rossby waves as the associated precipitation and circulation patterns suggest, which resemble tropical plumes (Figs. 1d and S1d). The relationship between the tropical and extratropical regime on the intraseasonal time scale is complex. One mechanism of how the MJO influences remote areas is through the excitation of Rossby wave trains (Opsteegh and van den Dool 1980; Hoskins and Karoly 1981; Seo and Lee 2017). During phase 4, precipitation is enhanced south of a trough located over the Atlas Mountains. The time lag composites prior to the tropical plume show that positive geopotential height anomalies are evident in the upper troposphere one month prior to rainfall events (Fig. 10a). In the Northern Hemisphere, a quasi-stationary Rossby wave train exists. The composites suggest that the MJO band rather reflects a standing than an eastward-propagating mode. A dry anomaly persists over Africa for several weeks and vanishes as soon as the geopotential anomaly vanishes. Related to the Rossby wave train over the Atlantic Ocean, the SHL is strengthened ahead of a ridge over Central Europe (Figs. 10a–c). The blocking frequency over the Atlantic Ocean and Europe has been shown to be modulated by the MJO (Henderson et al. 2016). Following this ridge, a trough amplifies over Central Europe 10 days later, which merges with a trough over the Atlas Mountains (Figs. 10e,f). The related southwesterlies over the Sahara transport moisture northward and facilitate the generation of rainfall over the region (Fig. 1d). Additionally to the geopotential anomalies over the Atlantic Ocean and Europe, a cyclonic and anticyclonic vortex pair exists over the Indian subcontinent 25–15 days before the event (Figs. 10a–c). This indicates a potential influence of the Indian monsoon system on the WAM on the intraseasonal time scale. The Indian monsoon system can influence the MJO signal over Africa during the monsoon season (Leroux et al. 2010; Berhane et al. 2015). Active and break phases of the Indian monsoon also project onto

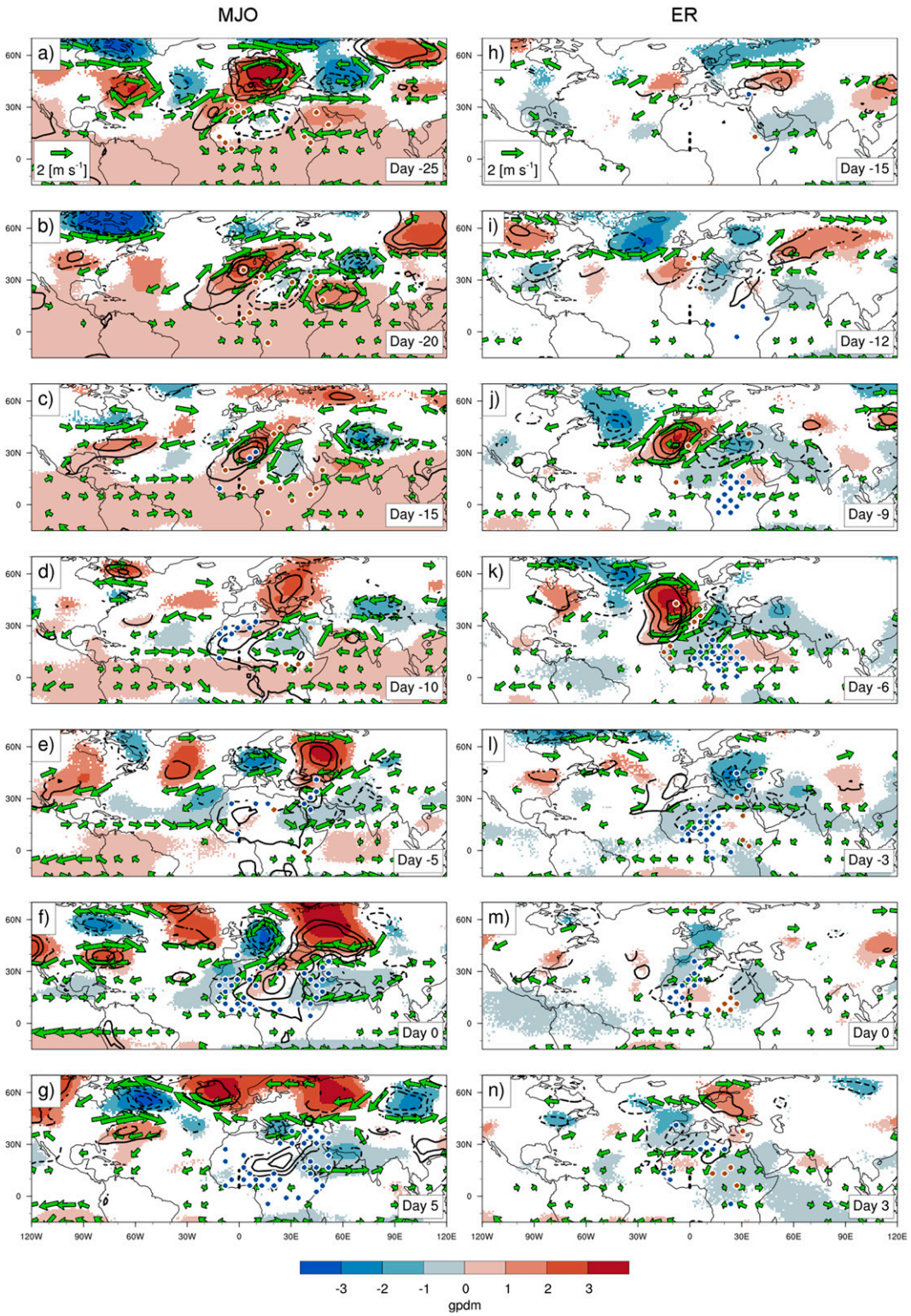

FIG. 10. Time lag composites of significant anomalies of wind (vector) and geopotential (shading) at 300 hPa and geopotential thickness between 925 and 600 hPa (contours; from −1 to 1 gpdm in steps of 0.25 gpdm; negative dashed) for days before the occurrence of (a)–(g) a tropical plumelike MJO signal during phase 4 and (h)–(n) an ER signal during phase 6. Significant precipitation anomalies over Africa are shown with blue (positive) and red (negative) dots. The wave signal was filtered for 5°–15°N, 0°E (dashed line). The analyzed time period spans from 1979 to 2013 for the extended monsoon season (March–October).

the intraseasonal signal of rainfall over West Africa 15–20 days later (Janicot et al. 2009). The quasi-stationarity of the signal in the extratropics suggests a possible link to other intraseasonal modes. The geopotential patterns at day −25 resemble a positive NAO pattern that reverses until day 0. Although, the AO is weak during boreal summer, a positive AO precedes the event, as negative geopotential anomalies in polar and positive anomalies in subtropical regions suggest. Time lag analysis of the NAO, AO, and PNA indices reveal that positive NAO and AO phases are more likely 40–20 days before the plume (Fig. 11). The NAO is related to intraseasonal variability over West Africa (Alaka and Maloney 2014) and the global MJO (Cassou 2008; Lin et al. 2009). The AO, which is correlated with the NAO, has been also associated with the MJO (Zhou and Miller 2005; L'Heureux and Higgins 2008). A connection with the PNA could not be found in this study, as has been noted for the global MJO previously (Ferranti et al. 1990; Mori and Watanabe 2008; Lukens et al. 2017), albeit for the boreal winter, whereas this study focuses on the premonsoon in late boreal spring.

ER waves, which act on a shorter time scale than the MJO, also show a precipitation pattern over the Sahara reminiscent of tropical plumes. The involved mechanism is likely different. Upper-level geopotential height patterns suggests that the westward-propagating ER signal interacts with the eastward movement of extratropical Rossby waves, triggering a wave breaking and leading to a tropical plume in phase 6 (not shown). Enhanced precipitation can then be found south and southeast of a trough over the Atlas Mountains. A similar pattern has been documented previously (Janicot et al. 2010; Thiawa et al. 2017). Twelve days before the event, weak geopotential anomaly patterns reach from the Atlantic Ocean to the Indian subcontinent, forming a Rossby wave train (Fig. 10i). As it intensifies, a ridge over western Europe triggers cold southeasterlies over northern Africa, which ventilate the northern part of the SHL. Over northern India, significant geopotential and thickness anomalies are evident at day −15 (Fig. 10h). These anomalies travel westward and intensify over central and East Africa (Figs. 10j,k). A trough, which stretches from the Atlas Mountains to Central Europe, strengthens and triggers northwesterly wind anomalies that subsequently lead to the formation of the tropical plume (Figs. 10l,m). Based on the time-lagged composites we hypothesize that breaking extratropical Rossby wave can project onto the ER band. From the time-lag analysis, it is not clear, however, to what portion ER waves can be attributed, that is, to an extratropical wave train or to tropical origin. Further research is needed here. Separating both regimes would help to answer this question.

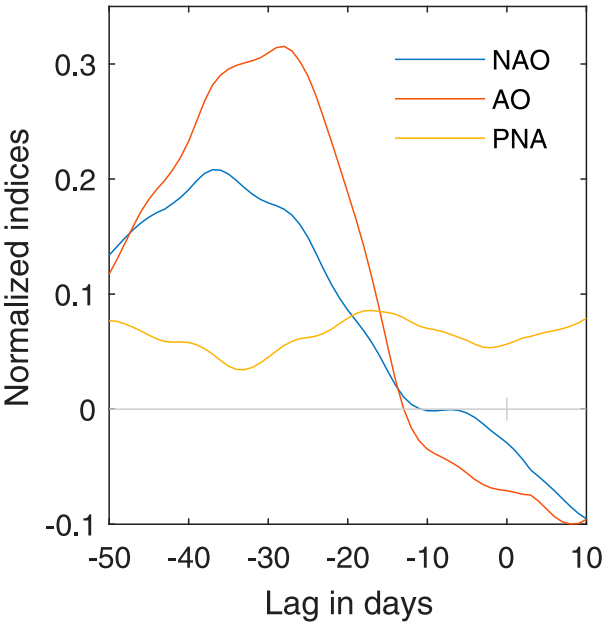

FIG. 11. Time lag analysis of mean NAO, AO, and PNA indices before significant MJO signals in local phase 4 at 0°E. A 15-day running mean was applied to the time series in order to highlight the intraseasonal variability.

As a final side remark, midlatitude wave trains originating over the Atlantic influence the intraseasonal variability of the WAM (Vizy and Cook 2009, 2014; Chauvin et al. 2010; Leroux et al. 2011). The SHL serves as a link between the extratropics and tropics (Chauvin et al. 2010; Leroux et al. 2011; Roehrig et al. 2011). Consequently, the strength and location of the SHL affects the activity of AEWs and intraseasonal variability of rainfall over northern tropical Africa. These studies and the results presented here emphasize the relevance of extratropical forcing for the intraseasonal rainfall variability in the study region.

4. Conclusions

Precipitation and the necessary dynamic and thermodynamic conditions are known to vary systematically in space and time in tropical regions like Africa. Tropical waves are the main factor determining the atmospheric environmental conditions that facilitate or suppress precipitation on daily to monthly time scales. So far no systematic comparison has been performed to analyze these waves and their influence on rainfall, dynamics, and thermodynamics over the region of northern tropical Africa. The present study complements Part I in which we quantified the influence of tropical waves on rainfall over the region. This part investigated the effect on the

dynamics and thermodynamics within the WAM. The key results are as follows:

- Tropical waves show specific circulation patterns that are largely consistent with theoretical predictions. The slow modes, MJO and ER waves, have a strong impact on PW, whereas moisture convergence is the dominant factor for rainfall generation in the faster TDs, Kelvin waves, and MRG waves. Monsoonal inflow is increased during wet phases of the MJO and ER and MRG waves. Because of the slow speed of the MJO and ER waves and their influence on PW, they are the only wave types significantly modulating the zonal position of the ITD by up to 100–200 km. MRG waves are a distinct mode over Africa that is significantly different from AEWs with respect to its dynamics. The modulation by EIG waves is very weak.
- Radiosonde data reveal the vertical tilt of imbalanced wave modes (TDs, Kelvin waves, and partially the MRG waves). The balanced ER waves are not vertically tilted. Organization of MCSs is facilitated during the wet phases of the imbalanced modes, the MJO, TDs, and Kelvin waves. Slightly favorable conditions occur during the passage of MRG waves. MCS formation is hampered during the passage of the balanced ER mode. Rainfall triggered by ER waves is more likely generated by large moistening and stratiform lifting.
- The MJO and ER waves interact with the extratropics. A time-lag analysis suggests that in both cases an extratropical Rossby wave train causes a trough over the Atlas Mountains, which then triggers rainfall over the Sahara. Additional influence stems from intraseasonal variability of the Indian monsoon system. The extratropical Rossby wave signal is likely the result of the MJO, whereas the ER signal is partially triggered by a related extratropical Rossby wave train over the Atlantic and partially has tropical origin. Time-lag analysis indicates that the MJO event is likely preceded by a positive NAO and AO signals.

Several scientific questions remain open. This study highlighted the differences between the effect of imbalanced modes in the WAM region compared to balanced modes. Current global NWP models struggle to assimilate small-scale imbalanced modes (Žagar 2017). This stresses the need for new schemes such as those proposed by Žagar et al. (2005), Žagar (2012), and Žagar et al. (2016). This study only analyzed thermodynamic variables and did not explicitly consider individual diabatic processes such as radiation and latent heat release, which is left for further research. Finally, the teleconnection patterns for the MJO and ER waves documented here should be analyzed in more detail because of their potential as intraseasonal predictors for Sahelian rainfall during the premonsoon.

Future developments of rainfall prediction models can benefit from the results presented here. This study unveiled which dynamical processes need to be modeled realistically to represent the coupling between tropical waves and rainfall. Operational NWP forecasts are improving in the representation of tropical waves (Dias et al. 2018; Janiga et al. 2018). In particular, the large-scale modulation of winds and moisture by the MJO, the quasigeostrophic equatorial (and related extratropical) Rossby waves are predicted reasonably well on a time scale of 2–3 weeks (Grazzini and Vitart 2015; Li and Robertson 2015; Janiga et al. 2018; Tseng et al. 2018). However, as numerical models still struggle to represent mesoscale structures of organized convection, the modulating influence of smaller-scale imbalanced tropical waves on rainfall might be missed. This gap could be addressed by developing dynamical–statistical models that incorporate real-time filtered wave information from NWP models and observations (Wheeler and Weickmann 2001; Wheeler and Hendon 2004; Roundy et al. 2009; Janiga et al. 2018) as predictors for rainfall, potentially leading to better rainfall predictions over northern tropical Africa.

Acknowledgments. The research leading to these results has been accomplished within project C2 ''Prediction of wet and dry periods of the West African Monsoon'' of the Transregional Collaborative Research Center SFB/TRR 165 ''Waves to Weather'' funded by the German Science Foundation (DFG). We thank Tilmann Gneiting and Peter Vogel for discussions and comments on draft versions of the paper. We acknowledge Michael Riemer's idea to use a time-lag analysis to analyze the origin of the MJO and ER signal. The authors also thank various colleagues and weather services that have over the years contributed to the enrichment of the KASS-D database; special thanks go to Robert Redl and Benedikt Heyl for creating the IGRA2reader package. The authors also thank Roderick van der Linden for providing code that was further developed to filter the waves and create the composites. Finally, we thank George Kiladis and one anonymous reviewer whose comments helped to substantially improve this manuscript.

REFERENCES

Agustí-Panareda, A., and Coauthors, 2010a: The ECMWF re-analysis for the AMMA observational campaign. *Quart. J. Roy. Meteor. Soc.*, **136**, 1457–1472, https://doi.org/10.1002/qj.662.

——, A. Beljaars, C. Cardinali, I. Genkova, and C. Thorncroft, 2010b: Impacts of assimilating AMMA soundings on ECMWF

analyses and forecasts. *Wea. Forecasting*, **25**, 1142–1160, https://doi.org/10.1175/2010WAF2222370.1.

Alaka, G. J., and E. D. Maloney, 2012: The influence of the MJO on upstream precursors to African easterly waves. *J. Climate*, **25**, 3219–3236, https://doi.org/10.1175/JCLI-D-11-00232.1.

——, and ——, 2014: The intraseasonal variability of African easterly wave energetics. *J. Climate*, **27**, 6559–6580, https://doi.org/10.1175/JCLI-D-14-00146.1.

Berhane, F., B. Zaitchik, and H. S. Badr, 2015: The Madden–Julian oscillation's influence on spring rainy season precipitation over equatorial West Africa. *J. Climate*, **28**, 8653–8672, https://doi.org/10.1175/JCLI-D-14-00510.1.

Brown, R. G., and C. Zhang, 1997: Variability of midtropospheric moisture and its effect on cloud-top height distribution during TOGA COARE. *J. Atmos. Sci.*, **54**, 2760–2774, https://doi.org/10.1175/1520-0469(1997)054<2760:VOMMAI>2.0.CO;2.

Browning, K. A., and F. H. Ludlam, 1962: Airflow in convective storms. *Quart. J. Roy. Meteor. Soc.*, **88**, 117–135, https://doi.org/10.1002/qj.49708837602.

Buckle, C., 1996: *Weather and Climate in Africa*. Longman, 312 pp.

Cassou, C., 2008: Intraseasonal interaction between the Madden–Julian oscillation and the North Atlantic Oscillation. *Nature*, **455**, 523–527, https://doi.org/10.1038/nature07286.

Chauvin, F., R. Roehrig, and J.-P. Lafore, 2010: Intraseasonal variability of the Saharan heat low and its link with midlatitudes. *J. Climate*, **23**, 2544–2561, https://doi.org/10.1175/2010JCLI3093.1.

Cheng, Y. M., C. D. Thorncroft, and G. N. Kiladis, 2019: Two contrasting African easterly wave behaviors. *J. Atmos. Sci.*, https://doi.org/10.1175/JAS-D-18-0300.1, in press.

Corfidi, S. F., 2003: Cold pools and MCS propagation: Forecasting the motion of downwind-developing MCSs. *Wea. Forecasting*, **18**, 997–1017, https://doi.org/10.1175/1520-0434(2003)018<0997:CPAMPF>2.0.CO;2.

Dee, D. P., and Coauthors, 2011: The ERA-Interim reanalysis: Configuration and performance of the data assimilation system. *Quart. J. Roy. Meteor. Soc.*, **137**, 553–597, https://doi.org/10.1002/qj.828.

Delayen, K., and J.-I. Yano, 2008: Is asymptotic non-divergence of the large-scale tropical atmosphere consistent with equatorial wave theories? *Tellus*, **61A**, 491–497, https://doi.org/10.1111/j.1600-0870.2009.00404.x.

Dias, J., and O. Pauluis, 2009: Convectively coupled waves propagating along an equatorial ITCZ. *J. Atmos. Sci.*, **66**, 2237–2255, https://doi.org/10.1175/2009JAS3020.1.

——, M. Gehne, G. N. Kiladis, N. Sakaeda, P. Bechtold, and T. Haiden, 2018: Equatorial waves and the skill of NCEP and ECMWF numerical weather prediction systems. *Mon. Wea. Rev.*, **146**, 1763–1784, https://doi.org/10.1175/MWR-D-17-0362.1.

Durre, I., R. S. Vose, X. Yin, S. Applequist, and J. Arnfield, 2016: Integrated Global Radiosonde Archive (IGRA), version 2. NOAA, accessed 28 May 2018, https://data.noaa.gov/dataset/dataset/integrated-global-radiosonde-archive-igra-version-2.

Duvel, J. P., 1990: Convection over tropical Africa and the Atlantic Ocean during northern summer. Part II: Modulation by easterly waves. *Mon. Wea. Rev.*, **118**, 1855–1868, https://doi.org/10.1175/1520-0493(1990)118<1855:COTAAT>2.0.CO;2.

Eldridge, R. H., 1957: A synoptic study of West African disturbance lines. *Quart. J. Roy. Meteor. Soc.*, **83**, 303–314, https://doi.org/10.1002/qj.49708335704.

Elless, T. J., and R. D. Torn, 2018: African easterly wave forecast verification and its relation to convective errors within the ECMWF ensemble prediction system. *Wea. Forecasting*, **33**, 461–477, https://doi.org/10.1175/WAF-D-17-0130.1.

Engel, T., A. H. Fink, P. Knippertz, G. Pante, and J. Bliefernicht, 2017: Extreme precipitation in the West African cities of Dakar and Ouagadougou: Atmospheric dynamics and implications for flood risk assessments. *J. Hydrometeor.*, **18**, 2937–2957, https://doi.org/10.1175/JHM-D-16-0218.1.

Ferranti, L., T. N. Palmer, F. Molteni, and E. Klinker, 1990: Tropical–extratropical interaction associated with the 30–60 day oscillation and its impact on medium and extended range prediction. *J. Atmos. Sci.*, **47**, 2177–2199, https://doi.org/10.1175/1520-0469(1990)047<2177:TEIAWT>2.0.CO;2.

Fink, A. H., and A. Reiner, 2003: Spatiotemporal variability of the relation between African easterly waves and West African squall lines in 1998 and 1999. *J. Geophys. Res.*, **108**, 4332, https://doi.org/10.1029/2002JD002816.

Fröhlich, L., P. Knippertz, A. H. Fink, and E. Hohberger, 2013: An objective climatology of tropical plumes. *J. Climate*, **26**, 5044–5060, https://doi.org/10.1175/JCLI-D-12-00351.1.

Funk, C., and Coauthors, 2015: The climate hazards infrared precipitation with stations—A new environmental record for monitoring extremes. *Sci. Data*, **2**, 150066, https://doi.org/10.1038/sdata.2015.66.

Gill, A. E., 1980: Some simple solutions for heat-induced tropical circulation. *Quart. J. Roy. Meteor. Soc.*, **106**, 447–462, https://doi.org/10.1002/qj.49710644905.

Grazzini, F., and F. Vitart, 2015: Atmospheric predictability and Rossby wave packets. *Quart. J. Roy. Meteor. Soc.*, **141**, 2793–2802, https://doi.org/10.1002/qj.2564.

Henderson, S. A., E. D. Maloney, and E. A. Barnes, 2016: The influence of the Madden–Julian oscillation on Northern Hemisphere winter blocking. *J. Climate*, **29**, 4597–4616, https://doi.org/10.1175/JCLI-D-15-0502.1.

Holder, C. T., S. E. Yuter, A. H. Sobel, and A. R. Aiyyer, 2008: The mesoscale characteristics of tropical oceanic precipitation during Kelvin and mixed Rossby–gravity wave events. *Mon. Wea. Rev.*, **136**, 3446–3464, https://doi.org/10.1175/2008MWR2350.1.

Hoskins, B. J., and D. J. Karoly, 1981: The steady linear response of a spherical atmosphere to thermal and orographic forcing. *J. Atmos. Sci.*, **38**, 1179–1196, https://doi.org/10.1175/1520-0469(1981)038<1179:TSLROA>2.0.CO;2.

Houze, R. A., 2004: Mesoscale convective systems. *Rev. Geophys.*, **42**, 86, https://doi.org/10.1029/2004RG000150.

Jalloh, A., M. D. Faye, H. Roy-Macauley, P. Sérémé, R. Zougmoré, T. S. Thomas, and G. C. Nelson, 2013: Overview. *West African Agriculture and Climate Change: A Comprehensive Analysis*, *IFPRI Research Monogr.*, IFPRI, 1–3.

Janicot, S., F. Mounier, N. M. J. Hall, S. Leroux, B. Sultan, and G. N. Kiladis, 2009: Dynamics of the West African monsoon. Part IV: Analysis of 25–90-day variability of convection and the role of the Indian monsoon. *J. Climate*, **22**, 1541–1565, https://doi.org/10.1175/2008JCLI2314.1.

——, ——, S. Gervois, B. Sultan, and G. N. Kiladis, 2010: The dynamics of the West African monsoon. Part V: The detection and role of the dominant modes of convectively coupled equatorial Rossby waves. *J. Climate*, **23**, 4005–4024, https://doi.org/10.1175/2010JCLI3221.1.

——, and Coauthors, 2011: Intraseasonal variability of the West African monsoon. *Atmos. Sci. Lett.*, **12**, 58–66, https://doi.org/10.1002/asl.280.

Janiga, M. A., and C. D. Thorncroft, 2016: The influence of African easterly waves on convection over tropical Africa and the East Atlantic. *Mon. Wea. Rev.*, **144**, 171–192, https://doi.org/10.1175/MWR-D-14-00419.1.

——, C. J. Schreck, J. A. Ridout, M. Flatau, N. P. Barton, E. J. Metzger, and C. A. Reynolds, 2018: Subseasonal forecasts of convectively coupled equatorial waves and the MJO: Activity and predictive skill. *Mon. Wea. Rev.*, **146**, 2337–2360, https://doi.org/10.1175/MWR-D-17-0261.1.

Jiang, X., and Coauthors, 2015: Vertical structure and physical processes of the Madden–Julian oscillation: Exploring key model physics in climate simulations. *J. Geophys. Res.*, **120**, 4718–4748, https://doi.org/10.1002/2014JD022375.

Kiladis, G. N., and M. Wheeler, 1995: Horizontal and vertical structure of observed tropospheric equatorial Rossby waves. *J. Geophys. Res.*, **100**, 22 981–22 997, https://doi.org/10.1029/95JD02415.

——, C. D. Thorncroft, and N. M. J. Hall, 2006: Three-dimensional structure and dynamics of African easterly waves. Part I: Observations. *J. Atmos. Sci.*, **63**, 2212–2230, https://doi.org/10.1175/JAS3741.1.

——, M. C. Wheeler, P. T. Haertel, K. H. Straub, and P. E. Roundy, 2009: Convectively coupled equatorial waves. *Rev. Geophys.*, **47**, RG2003, https://doi.org/10.1029/2008RG000266.

——, J. Dias, and M. Gehne, 2016: The relationship between equatorial mixed Rossby–gravity and eastward inertio-gravity waves. Part I. *J. Atmos. Sci.*, **73**, 2123–2145, https://doi.org/10.1175/JAS-D-15-0230.1.

Knippertz, P., 2003: Tropical–extratropical interactions causing precipitation in northwest Africa: Statistical analysis and seasonal variations. *Mon. Wea. Rev.*, **131**, 3069–3076, https://doi.org/10.1175/1520-0493(2003)131<3069:TICPIN>2.0.CO;2.

——, and J. E. Martin, 2005: Tropical plumes and extreme precipitation in subtropical and tropical West Africa. *Quart. J. Roy. Meteor. Soc.*, **131**, 2337–2365, https://doi.org/10.1256/qj.04.148.

——, A. H. Fink, A. Reiner, and P. Speth, 2003: Three late summer/early autumn cases of tropical–extratropical interactions causing precipitation in northwest Africa. *Mon. Wea. Rev.*, **131**, 116–135, https://doi.org/10.1175/1520-0493(2003)131<0116:TLSEAC>2.0.CO;2.

Lafore, J.-P., and Coauthors, 2017: A multi-scale analysis of the extreme rain event of Ouagadougou in 2009. *Quart. J. Roy. Meteor. Soc.*, **143**, 3094–3109, https://doi.org/10.1002/qj.3165.

Laing, A. G., J. M. Fritsch, and A. J. Negri, 1999: Contribution of mesoscale convective complexes to rainfall in Sahelian Africa: Estimates from geostationary infrared and passive microwave data. *J. Appl. Meteor.*, **38**, 957–964, https://doi.org/10.1175/1520-0450(1999)038<0957:COMCCT>2.0.CO;2.

——, R. E. Carbone, and V. Levizzani, 2011: Cycles and propagation of deep convection over equatorial Africa. *Mon. Wea. Rev.*, **139**, 2832–2853, https://doi.org/10.1175/2011MWR3500.1.

Lavaysse, C., A. Diedhiou, H. Laurent, and T. Lebel, 2006: African easterly waves and convective activity in wet and dry sequences of the West African monsoon. *Climate Dyn.*, **27**, 319–332, https://doi.org/10.1007/s00382-006-0137-5.

——, C. Flamant, S. Janicot, D. J. Parker, J.-P. Lafore, B. Sultan, and J. Pelon, 2009: Seasonal evolution of the West African heat low: A climatological perspective. *Climate Dyn.*, **33**, 313–330, https://doi.org/10.1007/s00382-009-0553-4.

——, ——, and ——, 2010: Regional-scale convection patterns during strong and weak phases of the Saharan heat low. *Atmos. Sci. Lett.*, **11**, 255–264, https://doi.org/10.1002/asl.284.

Lavender, S. L., and A. J. Matthews, 2009: Response of the West African monsoon to the Madden–Julian oscillation. *J. Climate*, **22**, 4097–4116, https://doi.org/10.1175/2009JCLI2773.1.

Lélé, I. M., and P. J. Lamb, 2010: Variability of the intertropical front (ITF) and rainfall over the West African Sudan–Sahel zone. *J. Climate*, **23**, 3984–4004, https://doi.org/10.1175/2010JCLI3277.1.

Leroux, S., N. M. J. Hall, and G. N. Kiladis, 2010: A climatological study of transient-mean-flow interactions over West Africa. *Quart. J. Roy. Meteor. Soc.*, **136**, 397–410, https://doi.org/10.1002/qj.474.

——, ——, and ——, 2011: Intermittent African easterly wave activity in a dry atmospheric model: Influence of the extratropics. *J. Climate*, **24**, 5378–5396, https://doi.org/10.1175/JCLI-D-11-00049.1.

L'Heureux, M. L., and R. W. Higgins, 2008: Boreal winter links between the Madden–Julian oscillation and the Arctic Oscillation. *J. Climate*, **21**, 3040–3050, https://doi.org/10.1175/2007JCLI1955.1.

Li, S., and A. W. Robertson, 2015: Evaluation of submonthly precipitation forecast skill from global ensemble prediction systems. *Mon. Wea. Rev.*, **143**, 2871–2889, https://doi.org/10.1175/MWR-D-14-00277.1.

Liebmann, B., and C. A. Smith, 1996: Description of a complete (interpolated) outgoing longwave radiation dataset. *Bull. Amer. Meteor. Soc.*, **77**, 1275–1277, https://doi.org/10.1175/1520-0477-77.6.1274.

Lin, H., G. Brunet, and J. Derome, 2009: An observed connection between the North Atlantic Oscillation and the Madden–Julian oscillation. *J. Climate*, **22**, 364–380, https://doi.org/10.1175/2008JCLI2515.1.

Lukens, K. E., S. B. Feldstein, C. Yoo, and S. Lee, 2017: The dynamics of the extratropical response to Madden–Julian Oscillation convection. *Quart. J. Roy. Meteor. Soc.*, **143**, 1095–1106, https://doi.org/10.1002/qj.2993.

Madden, R. A., and P. R. Julian, 1971: Detection of a 40–50 day oscillation in the zonal wind in the tropical Pacific. *J. Atmos. Sci.*, **28**, 702–708, https://doi.org/10.1175/1520-0469(1971)028<0702:DOADOI>2.0.CO;2.

Mapes, B., S. Tulich, J. Lin, and P. Zuidema, 2006: The mesoscale convection life cycle: Building block or prototype for large-scale tropical waves? *Dyn. Atmos. Oceans*, **42**, 3–29, https://doi.org/10.1016/j.dynatmoce.2006.03.003.

Maranan, M., A. H. Fink, and P. Knippertz, 2018: Rainfall types over southern West Africa: Objective identification, climatology and synoptic environment. *Quart. J. Roy. Meteor. Soc.*, **144**, 1628–1648, https://doi.org/10.1002/qj.3345.

Matsuno, T., 1966: 1966: Quasi-geostrophic motions in the equatorial area. *J. Meteor. Soc. Japan*, **44**, 25–44, https://doi.org/10.2151/jmsj1965.44.1_25.

Matthews, A. J., 2004: Intraseasonal variability over tropical Africa during northern summer. *J. Climate*, **17**, 2427–2440, https://doi.org/10.1175/1520-0442(2004)017<2427:IVOTAD>2.0.CO;2.

Mekonnen, A., and C. D. Thorncroft, 2016: On mechanisms that determine synoptic time scale convection over East Africa. *Int. J. Climatol.*, **36**, 4045–4057, https://doi.org/10.1002/joc.4614.

——, ——, and A. R. Aiyyer, 2006: Analysis of convection and its association with African easterly waves. *J. Climate*, **19**, 5405–5421, https://doi.org/10.1175/JCLI3920.1.

——, ——, ——, and G. N. Kiladis, 2008: Convectively coupled Kelvin waves over tropical Africa during the boreal summer: Structure and variability. *J. Climate*, **21**, 6649–6667, https://doi.org/10.1175/2008JCLI2008.1.

Moncrieff, M. W., and M. J. Miller, 1976: The dynamics and simulation of tropical cumulonimbus and squall lines. *Quart. J. Roy. Meteor. Soc.*, **102**, 373–394, https://doi.org/10.1002/qj.49710243208.

Mori, M., and M. Watanabe, 2008: The growth and triggering mechanisms of the PNA: A MJO–PNA coherence. *J. Meteor. Soc. Japan*, **86**, 213–236, https://doi.org/10.2151/jmsj.86.213.

Mounier, F., G. N. Kiladis, and S. Janicot, 2007: Analysis of the dominant mode of convectively coupled Kelvin waves in the West African monsoon. *J. Climate*, **20**, 1487–1503, https://doi.org/10.1175/JCLI4059.1.

Nguyen, H., and J.-P. Duvel, 2008: Synoptic wave perturbations and convective systems over equatorial Africa. *J. Climate*, **21**, 6372–6388, https://doi.org/10.1175/2008JCLI2409.1.

Nicholls, S. D., and K. I. Mohr, 2010: An analysis of the environments of intense convective systems in West Africa in 2003. *Mon. Wea. Rev.*, **138**, 3721–3739, https://doi.org/10.1175/2010MWR3321.1.

Opsteegh, J. D., and H. M. van den Dool, 1980: Seasonal differences in the stationary response of a linearized primitive equation model: Prospects for long-range weather forecasting? *J. Atmos. Sci.*, **37**, 2169–2185, https://doi.org/10.1175/1520-0469(1980)037<2169:SDITSR>2.0.CO;2.

Pohl, B., S. Janicot, B. Fontaine, and R. Marteau, 2009: Implication of the Madden–Julian oscillation in the 40-day variability of the West African monsoon. *J. Climate*, **22**, 3769–3785, https://doi.org/10.1175/2009JCLI2805.1.

Rasmussen, L. V., O. Mertz, K. Rasmussen, H. Nieto, A. Ali, and I. Maiga, 2014: Weather, climate, and resource information should meet the needs of Sahelian pastoralists. *Wea. Climate Soc.*, **6**, 482–494, https://doi.org/10.1175/WCAS-D-14-00010.1.

Raymond, D. J., and H. Jiang, 1990: A theory for long-lived mesoscale convective systems. *J. Atmos. Sci.*, **47**, 3067–3077, https://doi.org/10.1175/1520-0469(1990)047<3067:ATFLLM>2.0.CO;2.

Reed, R. J., D. C. Norquist, and E. E. Recker, 1977: The structure and properties of African wave disturbances as observed during phase III of GATE. *Mon. Wea. Rev.*, **105**, 317–333, https://doi.org/10.1175/1520-0493(1977)105<0317:TSAPOA>2.0.CO;2.

Riehl, H., 1945: *Waves in the Easterlies and the Polar Front in the Tropics*. 2nd ed. Vol. 17, Miscellaneous Reports, Department of Meteorology, University of Chicago, University of Chicago Press, 79 pp.

——, 1950: On the role of the tropics in the general circulation of the atmosphere. *Tellus*, **2**, 1–17, https://doi.org/10.3402/tellusa.v2i1.8531.

Riley, E. M., B. E. Mapes, and S. N. Tulich, 2011: Clouds associated with the Madden–Julian oscillation: A new perspective from *CloudSat*. *J. Atmos. Sci.*, **68**, 3032–3051, https://doi.org/10.1175/JAS-D-11-030.1.

Roberts, A. J., J. H. Marsham, and P. Knippertz, 2015: Disagreements in low-level moisture between (re)analyses over summertime West Africa. *Mon. Wea. Rev.*, **143**, 1193–1211, https://doi.org/10.1175/MWR-D-14-00218.1.

Roca, R., J.-P. Lafore, C. Piriou, and J.-L. Redelsperger, 2005: Extratropical dry-air intrusions into the West African monsoon midtroposphere: An important factor for the convective activity over the Sahel. *J. Atmos. Sci.*, **62**, 390–407, https://doi.org/10.1175/JAS-3366.1.

Roehrig, R., F. Chauvin, and J.-P. Lafore, 2011: 10–25-day intraseasonal variability of convection over the Sahel: A role of the Saharan heat low and midlatitudes. *J. Climate*, **24**, 5863–5878, https://doi.org/10.1175/2011JCLI3960.1.

Rotunno, R., J. B. Klemp, and M. L. Weisman, 1988: A theory for strong, long-lived squall lines. *J. Atmos. Sci.*, **45**, 463–485, https://doi.org/10.1175/1520-0469(1988)045<0463:ATFSLL>2.0.CO;2.

Roudier, P., A. Alhassane, C. Baron, S. Louvet, and B. Sultan, 2016: Assessing the benefits of weather and seasonal forecasts to millet growers in Niger. *Agric. For. Meteor.*, **223**, 168–180, https://doi.org/10.1016/j.agrformet.2016.04.010.

Roundy, P. E., 2012: Observed structure of convectively coupled waves as a function of equivalent depth: Kelvin waves and the Madden–Julian oscillation. *J. Atmos. Sci.*, **69**, 2097–2106, https://doi.org/10.1175/JAS-D-12-03.1.

——, and W. M. Frank, 2004: A climatology of waves in the equatorial region. *J. Atmos. Sci.*, **61**, 2105–2132, https://doi.org/10.1175/1520-0469(2004)061<2105:ACOWIT>2.0.CO;2.

——, and M. A. Janiga, 2012: Analysis of vertically propagating convectively coupled equatorial waves using observations and a non-hydrostatic Boussinesq model on the equatorial beta-plane. *Quart. J. Roy. Meteor. Soc.*, **138**, 1004–1017, https://doi.org/10.1002/qj.983.

——, C. J. Schreck, and M. A. Janiga, 2009: Contributions of convectively coupled equatorial Rossby waves and Kelvin waves to the real-time multivariate MJO indices. *Mon. Wea. Rev.*, **137**, 469–478, https://doi.org/10.1175/2008MWR2595.1.

Schlueter, A., A. H. Fink, P. Knippertz, and P. Vogel, 2019: A systematic comparison of tropical waves over northern Africa. Part I: Influence on rainfall. *J. Climate*, 32, 1501–1523, https://doi.org/10.1175/JCLI-D-18-0173.1.

Schrage, J. M., A. H. Fink, V. Ermert, and E. D. Ahlonsou, 2006: Three MCS cases occurring in different synoptic environments in the sub-Sahelian wet zone during the 2002 West African monsoon. *J. Atmos. Sci.*, **63**, 2369–2382, https://doi.org/10.1175/JAS3757.1.

Seo, K.-H., and H.-J. Lee, 2017: Mechanisms for a PNA-like teleconnection pattern in response to the MJO. *J. Atmos. Sci.*, **74**, 1767–1781, https://doi.org/10.1175/JAS-D-16-0343.1.

Sinclaire, Z., A. Lenouo, C. Tchawoua, and S. Janicot, 2015: Synoptic Kelvin type perturbation waves over Congo basin over the period 1979–2010. *J. Atmos. Sol. Terr. Phys.*, **130–131**, 43–56, https://doi.org/10.1016/j.jastp.2015.04.015.

Stan, C., D. M. Straus, J. S. Frederiksen, H. Lin, E. D. Maloney, and C. Schumacher, 2017: Review of tropical–extratropical teleconnections on intraseasonal time scales. *Rev. Geophys.*, **55**, 902–937, https://doi.org/10.1002/2016RG000538.

Sultan, B., S. Janicot, and A. Diedhiou, 2003: The West African monsoon dynamics. Part I: Documentation of intraseasonal variability. *J. Climate*, **16**, 3389–3406, https://doi.org/10.1175/1520-0442(2003)016<3389:TWAMDP>2.0.CO;2.

Takayabu, Y. N., and T. Nitta, 1993: 3-5 day-period disturbances coupled with convection over the tropical Pacific Ocean. J. Meteor. Soc. Japan. *Ser. II*, **71**, 221–246, https://doi.org/10.2151/jmsj1965.71.2_221.

Thiawa, W. M., and Coauthors, 2017: Subseasonal forecasting. *Meteorology of Tropical West Africa: The Forecaster's Handbook*, D. J. Parker, and M. Diop-Kane, Eds., John Wiley & Sons, 255–288.

Thompson, D. W. J., and J. M. Wallace, 1998: The Arctic oscillation signature in the wintertime geopotential height and temperature fields. *Geophys. Res. Lett.*, **25**, 1297–1300, https://doi.org/10.1029/98GL00950.

Tian, B., D. E. Waliser, E. J. Fetzer, B. H. Lambrigtsen, Y. L. Yung, and B. Wang, 2006: Vertical moist thermodynamic structure and spatial–temporal evolution of the MJO in AIRS observations. *J. Atmos. Sci.*, **63**, 2462–2485, https://doi.org/10.1175/JAS3782.1.

Tseng, K.-C., E. A. Barnes, and E. D. Maloney, 2018: Prediction of the midlatitude response to strong Madden–Julian oscillation events on S2S time scales. *Geophys. Res. Lett.*, **45**, 463–470, https://doi.org/10.1002/2017GL075734.

Ventrice, M. J., and C. D. Thorncroft, 2013: The role of convectively coupled atmospheric Kelvin waves on African easterly wave

activity. *Mon. Wea. Rev.*, **141**, 1910–1924, https://doi.org/10.1175/MWR-D-12-00147.1.

——, ——, and P. E. Roundy, 2011: The Madden–Julian oscillation's influence on African easterly waves and downstream tropical cyclogenesis. *Mon. Wea. Rev.*, **139**, 2704–2722, https://doi.org/10.1175/MWR-D-10-05028.1.

Vitart, F., and A. W. Robertson, 2018: The sub-seasonal to seasonal prediction project (S2S) and the prediction of extreme events. *npj Climate Atmos. Sci.*, **1**, 3549, https://doi.org/10.1038/s41612-018-0013-0.

Vizy, E. K., and K. H. Cook, 2009: A mechanism for African monsoon breaks: Mediterranean cold air surges. *J. Geophys. Res.*, **114**, D01104, https://doi.org/10.1029/2008JD010654.

——, and ——, 2014: Impact of cold air surges on rainfall variability in the Sahel and wet African tropics: A multi-scale analysis. *Climate Dyn.*, **43**, 1057–1081, https://doi.org/10.1007/s00382-013-1953-z.

Vogel, P., P. Knippertz, A. H. Fink, A. Schlueter, and T. Gneiting, 2018: Skill of global raw and postprocessed ensemble predictions of rainfall over northern tropical Africa. *Wea. Forecasting*, **33**, 369–388, https://doi.org/10.1175/WAF-D-17-0127.1.

Waliser, D. E., K. M. Lau, W. Stern, and C. Jones, 2003: Potential predictability of the Madden–Julian oscillation. *Bull. Amer. Meteor. Soc.*, **84**, 33–50, https://doi.org/10.1175/BAMS-84-1-33.

Walker, G., and E. Bliss, 1932: World weather V. *Mem. Roy. Meteor. Soc.*, **36**, 53–84.

Wallace, J. M., and D. S. Gutzler, 1981: Teleconnections in the geopotential height field during the Northern Hemisphere winter. *Mon. Wea. Rev.*, **109**, 784–812, https://doi.org/10.1175/1520-0493(1981)109<0784:TITGHF>2.0.CO;2.

Wheeler, M., and G. N. Kiladis, 1999: Convectively coupled equatorial waves: Analysis of clouds and temperature in the wavenumber–frequency domain. *J. Atmos. Sci.*, **56**, 374–399, https://doi.org/10.1175/1520-0469(1999)056<0374:CCEWAO>2.0.CO;2.

——, and K. M. Weickmann, 2001: Real-time monitoring and prediction of modes of coherent synoptic to intraseasonal tropical variability. *Mon. Wea. Rev.*, **129**, 2677–2694, https://doi.org/10.1175/1520-0493(2001)129<2677:RTMAPO>2.0.CO;2.

——, and H. H. Hendon, 2004: An all-season real-time multivariate MJO index: Development of an index for monitoring and prediction. *Mon. Wea. Rev.*, **132**, 1917–1932, https://doi.org/10.1175/1520-0493(2004)132<1917:AARMMI>2.0.CO;2.

Yang, G.-Y., and B. J. Hoskins, 2017: The equivalent barotropic structure of waves in the tropical atmosphere in the Western Hemisphere. *J. Atmos. Sci.*, **74**, 1689–1704, https://doi.org/10.1175/JAS-D-16-0267.1.

——, J. Methven, S. Woolnough, K. Hodges, and B. Hoskins, 2018: Linking African easterly wave activity with equatorial waves and the influence of Rossby waves from the Southern Hemisphere. *J. Atmos. Sci.*, **75**, 1783–1809, https://doi.org/10.1175/JAS-D-17-0184.1.

Yasunaga, K., and B. Mapes, 2012: Differences between more divergent and more rotational types of convectively coupled equatorial waves. Part II: Composite analysis based on space–time filtering. *J. Atmos. Sci.*, **69**, 17–34, https://doi.org/10.1175/JAS-D-11-034.1.

Žagar, N., 2012: Multivariate data assimilation in the tropics by using equatorial waves. *Pure Appl. Geophys.*, **169**, 367–379, https://doi.org/10.1007/s00024-011-0375-2.

——, 2017: A global perspective of the limits of prediction skill of NWP models. *Tellus*, **69A**, 1317573, https://doi.org/10.1080/16000870.2017.1317573.

——, E. Andersson, and M. Fisher, 2005: Balanced tropical data assimilation based on a study of equatorial waves in ECMWF short-range forecast errors. *Quart. J. Roy. Meteor. Soc.*, **131**, 987–1011, https://doi.org/10.1256/qj.04.54.

——, M. Blaauw, B. Jesenko, and L. Magnusson, 2016: Diagnosing model performance in the tropics. *ECMWF Newsletter*, No. 147, ECMWF, Reading, United Kingdom, 26–33.

Zaitchik, B. F., 2017: Madden–Julian oscillation impacts on tropical African precipitation. *Atmos. Res.*, **184**, 88–102, https://doi.org/10.1016/j.atmosres.2016.10.002.

Zhang, C., 2005: Madden–Julian Oscillation. *Rev. Geophys.*, **43**, RG2003, https://doi.org/10.1029/2004RG000158.

——, 2013: Madden–Julian oscillation: Bridging weather and climate. *Bull. Amer. Meteor. Soc.*, **94**, 1849–1870, https://doi.org/10.1175/BAMS-D-12-00026.1.

Zhou, S., and A. J. Miller, 2005: The interaction of the Madden–Julian oscillation and the Arctic Oscillation. *J. Climate*, **18**, 143–159, https://doi.org/10.1175/JCLI3251.1.

Zipser, E. J., 1977: Mesoscale and convective–scale downdrafts as distinct components of squall-line structure. *Mon. Wea. Rev.*, **105**, 1568–1589, https://doi.org/10.1175/1520-0493(1977)105<1568:MACDAD>2.0.CO;2.